



Published in final edited form as:

Nanotoxicology. 2013 November ; 7(7): 1179–1194. doi:10.3109/17435390.2012.719649.

## Acute pulmonary dose–responses to inhaled multi-walled carbon nanotubes

Dale W. Porter<sup>1,2</sup>, Ann F. Hubbs<sup>1</sup>, Bean T. Chen<sup>1</sup>, Walter McKinney<sup>1</sup>, Robert R. Mercer<sup>1,2</sup>, Michael G. Wolfarth<sup>1</sup>, Lori Battelli<sup>1</sup>, Nianqiang Wu<sup>3</sup>, Krishnan Sriram<sup>1</sup>, Stephen Leonard<sup>1</sup>, Michael Andrew<sup>1</sup>, Patsy Willard<sup>1</sup>, Shuji Tsuruoka<sup>4</sup>, Morinobu Endo<sup>4</sup>, Takayuki Tsukada<sup>5</sup>, Fuminori Mune Kane<sup>5</sup>, David G. Frazer<sup>1,2</sup>, and Vincent Castranova<sup>1</sup>

<sup>1</sup>National Institute for Occupational Safety and Health, Morgantown, WV, USA

<sup>2</sup>Department of Physiology and Pharmacology, West Virginia University, Morgantown, WV, USA

<sup>3</sup>Department of Mechanical & Aerospace Engineering, West Virginia University, Morgantown, WV, USA

<sup>4</sup>Research Center for Exotic Nanocarbons, Shinshu University, 4-17-1 Wakasato, Nagano-shi, Japan

<sup>5</sup>Hodogaya Chemical Company, LTD. 2-4-1 Yaesu, Chuo-Ku, Tokyo, Japan

### Abstract

This study investigated the *in vivo* pulmonary toxicity of inhaled multi-walled carbon nanotubes (MWCNT). Mice-inhaled aerosolized MWCNT (10 mg/m<sup>3</sup>, 5 h/day) for 2, 4, 8 or 12 days. MWCNT lung burden was linearly related to exposure duration. MWCNT-induced pulmonary inflammation was assessed by determining whole lung lavage (WLL) polymorphonuclear leukocytes (PMN). Lung cytotoxicity was assessed by WLL fluid LDH activities. WLL fluid albumin concentrations were determined as a marker of alveolar air–blood barrier integrity. These parameters significantly increased in MWCNT-exposed mice versus controls and were dose-dependent. Histopathologic alterations identified in the lung included (1) bronchiolocentric inflammation, (2) bronchiolar epithelial hyperplasia and hypertrophy, (3) fibrosis, (4) vascular changes and (5) rare pleural penetration. MWCNT translocated to the lymph node where the deep paracortex was expanded after 8 or 12 days. Acute inhalation of MWCNT induced dose-dependent pulmonary inflammation and damage with rapid development of pulmonary fibrosis, and also demonstrated that MWCNT can reach the pleura after inhalation exposure.

Correspondence: Dale W. Porter, PhD, Pathology and Physiology Research Branch, Health Effects Laboratory Division, National Institute for Occupational Safety and Health, 1095 Willowdale Road, M/S 2015, Morgantown, WV, 26505, USA. Tel: +1 304 285 6320. Fax: +1 304 285 6389. DPorter@cdc.gov.

### Declaration of interest

This work was supported by NIOSH Nanotechnology Research Center (Project 2927ZKKV, Toxicological Effects of Aerosolized MWCNT). Morinobu Endo was supported by a Grant-in-Aid for Specially Promoted Research from the Ministry of Education, Culture, Sports, Science and Technology of Japan (MEXT) (No. 19002007). Shuji Tsuruoka and Morinobu Endo were supported by the Exotic Nanocarbon Project, Japan Regional Innovation Strategy Program by the Excellence, JST (Japan Science and Technology Agency). Takayuki Tsukada and Fuminori Mune Kane are employed by Hodogaya Chemical Company, the manufacturer of the MWCNT used in this study. The authors report no conflicts of interest. The authors alone are responsible for the content and writing of this paper. The findings and conclusions in this report are those of the authors and do not necessarily represent the views of the National Institute for Occupational Safety and Health.

## Keywords

characterisation; lung burden; inflammation; fibrosis; pleural penetration

---

## Introduction

Several different multi-walled carbon nanotube (MWCNT) inhalation studies have reported various outcomes regarding the toxicity of MWCNT. One study reported no lung inflammation but did observe thickening of the alveolar septa after exposure of mice to MWCNT aerosol (32 mg/m<sup>3</sup>) for 8, 16 or 24 days (Li et al. 2007). A second study also reported that inhalation exposure of mice to MWCNT induced no significant tissue damage or inflammation, but alveolar macrophages (AM) contained black particles and there was systemic immunosuppression (Mitchell et al. 2007). Another MWCNT inhalation study compared the effect of MWCNT inhalation between normal and ovalbumin-sensitised mice (Ryman-Rasmussen et al. 2009a). In this study, mice were exposed to a MWCNT aerosol (100 mg/m<sup>3</sup>) for 6 h. Significant airway fibrosis was evident at 14 days post-exposure, but only in ovalbumin-sensitised mice, which led the authors of this study to conclude that inhaled MWCNT require pre-existing inflammation to cause airway fibrosis. Rats exposed to MWCNT aerosols up to 2.5 mg/m<sup>3</sup> for 13 weeks showed multifocal granulomatous inflammation, diffuse histiocytic and neutrophilic inflammation, and intra-alveolar lipoproteinosis (Ma-Hock et al. 2009), while another 13-week inhalation study of rats exposed to MWCNT reported persistent pulmonary inflammation and granulomas in rats exposed to 0.4–6 mg/m<sup>3</sup> (Pauluhn 2010).

Previous studies from our laboratory have reported extensively on the *in vivo* toxicity of MWCNT after pharyngeal aspiration exposure. Aspiration exposure of mice to MWCNT resulted in dose- and time-dependent pulmonary inflammation and damage at lung burdens approximating feasible human occupational exposures to MWCNT (Porter et al. 2010). In addition, MWCNT aspiration caused rapid fibrosis, persistent granulomatous inflammation, hypertrophy and hyperplasia of bronchiolar epithelium, mucous metaplasia of the bronchiolar epithelium, and at the highest exposures in the 56-day post-exposure time point, peribronchiolar lymphatics were dilated (Porter et al. 2010). In addition, MWCNT were observed penetrating the pleura (Porter et al. 2010). Next, morphometric measurements were used to investigate the distribution of MWCNT and the number of MWCNT penetrations of the alveolar epithelium, subpleural tissue defined as the alveolar epithelium immediately adjacent to the pleura, and intrapleural space defined as visceral pleural surface (Mercer et al. 2010). This study determined that at 56 days post-exposure, approximately one in every 400 MWCNT was in either the subpleural tissue or intrapleural space, and numerous penetrations into macrophages in the alveolar airspaces were found at all post-exposure times. A recent report used morphometry to determine that the average thickness of connective tissue in the alveolar septa was increased over vehicle control by 45% in the 40 µg and 73% in the 80 µg exposure groups at 56 days post-exposure, demonstrating that MWCNT have the potential to produce a progressive, fibrotic response in the alveolar tissues of the lungs (Mercer et al. 2011). Also, using Ingenuity Pathway Analysis (IPA), we determined that MWCNT exposure affects a subset of lung cancer biomarkers and identified

several carcinogenic-related signalling pathways that may be involved in the response (Pacurari et al. 2011). These studies, when considered together, provide compelling evidence that MWCNT may pose a significant human health risk.

In the present study, we continue our investigation of MWCNT *in vivo* lung toxicity by conducting an inhalation study. Specifically, mice were exposed to aerosolized MWCNT (10 mg/m<sup>3</sup>, 5 h/day) for 2, 4, 8 or 12 days, and pulmonary inflammation, damage and fibrosis were assessed at 1 day post-exposure. In addition, we measured lung burden and evaluated histopathologic changes in the nose, lung and tracheobronchial lymph node.

## Materials and methods

### MWCNT

MWCNT used in this study were obtained from Hodogaya Chemical Company (MWNT-7, lot #061220-31) and were manufactured using a floating reactant catalytic chemical vapour deposition method followed by high-temperature thermal treatment in argon at 2500°C using a continuous furnace (Kim et al. 2005).

### High-resolution transmission electron microscopy

The MWCNT were observed under Philips CM 20 transmission electron microscope (TEM) equipped with EDS (EDAX/4pi). To prepare the TEM specimens, the MWCNT were dispersed into ethanol with the assistance of sonication. A droplet of this MWCNT suspension was then pipetted onto a carbon-coated copper grid and subsequently dried in ambient air at room temperature prior to TEM observation.

### MWCNT trace metal analyses

To determine trace metals, bulk samples of MWCNT were digested by the nitric/perchloric acid ashing procedure (NIOSH 1994). The residues were dissolved in 10.0 ml of 4% HNO<sub>3</sub>-1% HClO<sub>4</sub> for trace metals analysis by inductively coupled plasma-optical emission spectroscopy.

### MWCNT endotoxin analyses

To determine endotoxin, bulk samples of MWCNT were prepared as 1.8 mg/ml suspensions in water. After rocking on a platform at room temperature for 24 h, the samples were centrifuged (5000 × g, 10 min, room temperature). Next, the samples were filtered using a 0.45 µm syringe filter to remove any remaining particulate. Endotoxin analyses were done using the Limulus amebocyte lysate assay (Kinetic-QCL, BioWhittaker, Walkersville, MD).

### XPS analyses of MWCNT

X-ray photoelectron spectroscopy (XPS) analyses were carried out with a PHI 5000 Versa Probe (Physical Electronics, MN). Prior to XPS measurement, the MWCNT were pressed to form a pellet. The pellet was then placed into the entry-load chamber and held in vacuum for 6 h. A monochromated Al K radiation (1486.6 eV) was employed as X-ray source. Survey scans and high-resolution scans were collected at the pass energies of 94 and 58 eV,

respectively. The binding energies of spectra were referenced to the C 1s binding energy at 284.6 eV for the carbon nanotubes.

### ESR analyses of MWCNT

All ESR measurements were conducted using a Bruker Instruments (Billerica, MA) EMX ESR spectrometer and a flat cell assembly. Hyperfine couplings were measured (to 0.1 G) directly from magnetic field separation using potassium tetraperoxochromate ( $K_3CrO_8$ ) and 1,1 diphenyl-2-picrylhydrazyl (DPPH) as reference standards. The Acquisit program (Bruker Instruments, Billerica, MA) was used for data acquisition and analysis. Each assay sample consisted of 100 mM 5,5-dimethyl-1-pyrroline-N-oxide (DMPO), 0.1 or 1 mM  $FeSO_4$ , 0.1 or 1 mM hydrogen peroxide ( $H_2O_2$ ) and  $\pm$  MWCNT (0.8 mg/ml) in a total volume of 1 ml of dispersion medium (Porter et al. 2008).

### Animals

Male C57BL/6J mice (6 weeks old) were obtained from Jackson Laboratories (Bar Harbor, ME). Mice were housed one per cage in polycarbonate isolator ventilated cages, which were provided HEPA-filtered air, with fluorescent lighting from 0700 to 1900 h. Autoclaved Alpha-Dri virgin cellulose chips and hardwood Beta-chips were used as bedding. Mice were monitored to be free of endogenous viral pathogens, parasites, mycoplasmas, *Helicobacter* and *CAR Bacillus*. Mice were maintained on Harlan Teklad Rodent Diet 7913 (Indianapolis, IN), and tap water was provided *ad libitum*. Animals were allowed to acclimate for at least 5 days before use. All animals used in this study were housed in an AAALAC-accredited, specific pathogen-free, environmentally controlled facility. All procedures involving animals were approved by the NIOSH Institutional Animal Care and Use Committee.

### MWCNT inhalation exposure and aerosol characterisation

Mice were exposed to a MWCNT aerosol ( $10 \text{ mg/m}^3$ , 5 h/day) for either 2, 4, 8 or 12 days, using an acoustical-based computer-controlled whole-body inhalation system designed and constructed by our laboratory (McKinney et al. 2009). In brief, the inhalation exposure system combines air flow controllers, aerosol particle monitors, data acquisition devices and custom software with automated feedback control to achieve constant and repeatable exposure chamber temperature, relative humidity, pressure, aerosol concentration and particle size distributions. The generator produces airborne particles continuously for long periods of time, e.g., 35 h of continuous operation, with minimal fluctuations during an exposure period. The uniformity of test atmosphere in the chamber was evaluated to have a total variation of  $<5\%$ . In this study, the MWCNT aerosol mass concentration was continuously monitored with a Data RAM (DR-40000 Thermo Electron Co, Franklin, MA), and gravimetric determinations (37 mm cassettes with  $0.45 \mu\text{m}$  pore-size Teflon filters) were used to calibrate and verify the Data RAM readings. In addition, a cascade impactor (MOUDI, Models 110 and 115, MSP Co., Shoreview, MN) was used to determine the mass- and number-based particle size distributions by fractionating the particles into 15 size fractions ranging from 10 nm to  $18 \mu\text{m}$ . Particle morphology was also evaluated from Nucleopore polycarbonate filters (Whatman, Clinton, PA) obtained from the cascade impactor.

### MWCNT lung burden

MWCNT burden determination method was based on modification to a previous method for the determination of mouse and rat lung carbon black (Elder et al. 2005). After euthanasia, lungs were removed and wet weights obtained. The lung tissue was digested in 25% KOH/methanol (w/v) at 60°C overnight, followed by centrifugation at  $16,000 \times g$  for 10 min. The supernatant was removed, the remaining pellet was mixed with 50% HNO<sub>3</sub>/methanol (v/v), and incubated at 60°C overnight, followed by centrifugation ( $16,000 \times g$ , 10 min). The supernatant was removed, and the pellet resuspended in 10% NP-40 (v/v) in dH<sub>2</sub>O, followed by 30-sec sonication using a probe sonicator. MWCNT standards were processed in parallel with the lung samples. The optical densities of the solutions were measured at 700 nm using a UV/visible spectrophotometer. Lung MWCNT content was determined from a standard curve.

### Whole lung lavage

At 1 day post-exposure, mice were euthanised with an i.p. injection of sodium pentobarbital (>100 mg/kg body weight) followed by exsanguination. A tracheal cannula was inserted, and whole lung lavage (WLL) was performed through the cannula using ice-cold Ca<sup>2+</sup> and Mg<sup>2+</sup>-free phosphate buffered saline (PBS), pH 7.4, supplemented with 5.5 mM D-glucose. The first lavage (0.6 ml) was kept separate from the rest of the lavage fluid. Subsequent lavages, each with 1 ml of PBS, were performed until a total of 4 ml of lavage fluid was collected. WLL cells were isolated by centrifugation ( $650 \times g$ , 5 min, 4°C). An aliquot of the acellular supernatant from the first WLL (WLL fluid) was decanted and transferred to tubes for analysis of lactate dehydrogenase (LDH) and albumin. The acellular supernatants from the remaining lavage samples were decanted and discarded. WLL cells isolated from the first and subsequent lavages for the same mouse were pooled after resuspension in PBS, centrifuged a second time ( $650 \times g$ , 5 min, 4°C), and the supernatant decanted and discarded. The WLL cell pellet was then resuspended in PBS and placed on ice. Total WLL cell counts were obtained using a Coulter Multisizer 3 (Coulter Electronics, Hialeah, FL) and cytospin preparations of the WLL cells were made using a cytocentrifuge (Shandon Elliot Cytocentrifuge, London). The cytospin preparations were stained with modified Wright-Giemsa stain, and cell differentials were determined by light microscopy.

### WLL fluid LDH, albumin and cytokine measurement

WLL fluid albumin concentrations were determined as an indicator of the integrity of the alveolar air–blood barrier. WLL fluid albumin was determined colorimetrically at 628 nm based on albumin binding to bromocresol green, using a commercial assay kit (Sigma Chemical Company, St. Louis, Mo). WLL fluid LDH activities were evaluated as a marker of cytotoxicity. WLL fluid LDH activities were determined by monitoring the LDH-catalysed oxidation of lactate to pyruvate coupled with the reduction of NAD at 340 nm using a commercial assay kit (Roche Diagnostics Systems, Montclair, NJ). Both the WLL fluid albumin and LDH assays were conducted using a COBAS MIRA Plus (Roche Diagnostic Systems, Montclair, NJ). The chemokine KC, which is a neutrophil chemoattractant, was determined in first WLL fluid using a commercial ELISA assay kit (AushonBiosystems, Billerica, MA).

## Histopathology

Following euthanasia, the lung, tracheobronchial lymph node and nose were rapidly removed. The lung was fixed by airway inflation with 6 cc of 10% neutral buffered formalin. The tracheobronchial lymph node and the nose were immersion fixed in 10% neutral buffered formalin. The lung and lymph node were trimmed on the day of necropsy, processed overnight and embedded in paraffin. The nose was decalcified in 13% formic acid and sectioned at three levels as previously described (Herbert & Leininger 1999; Young 1981). A fourth level, further back in the nose, was included for a more complete assessment of nasal changes. Sections from the left lung lobe, tracheobronchial lymph node and nose were stained with hematoxylin and eosin for routine pathology evaluation. In addition, the sections of left lung lobe were stained with Masson's trichrome to evaluate fibrosis and with alcian blue/periodic acid-Schiff to evaluate mucosubstances (American Registry of Pathology 1968). Sections of lung and lymph node were examined at the 4-, 8- and 12-day time points, and sections of nose were examined at the 12-day time point.

Slides were interpreted by a board-certified veterinary pathologist (AFH). Semi-quantitative histopathology scores were assigned for major categories of lung and nose histopathology changes as previously described (Hubbs et al. 2008). In brief, a severity score was assigned to quantify the severity of the response (where none = 0, minimal = 1, mild = 2, moderate = 3, marked = 4 and severe = 5) and a distribution score was assigned to quantify how that change was distributed within the lung (where none = 0, focal = 1, locally extensive = 2, multifocal = 3, multifocal and coalescent = 4 and diffuse = 5). The pathology score was the sum of the severity and distribution scores. Due to the compartmental nature of hyperplasia and particle translocation in the tracheobronchial lymph node, only the severity score was used as a quantitative measure (where none = 0, minimal = 1, mild = 2, moderate = 3, marked = 4 and severe = 5) with a notation of the affected compartment where appropriate (e.g., paracortical). Cytopathologic changes associated with penetration of cellular membranes by MWCNT and phagocytosis of apoptotic cells were qualitatively evaluated at 100× magnification in hematoxylin and eosin-stained sections of lung, nose and lymph node.

## Augmented microscopic imaging

To further document MWCNT penetration of the pleura, H&E-stained sections from MWCNT-exposed mice in the 12-day time point were examined using enhanced-darkfield light microscopy using illumination optics designed for visualisation of refractive nanoparticles and an Olympus BX-41 microscope (CytoViva, Auburn, AL) as previously described (Mercer et al. 2011). Enhanced-darkfield light microscopy was also used for visualisation of cells obtained by WLL from MWCNT-exposed mice at the 12-day time point.

Additional sections of the left lung lobe from the 12-day time point were stained with ethidium homodimer-1, a nucleic acid stain, and for lamin B1, a nuclear membrane protein and imaged by confocal microscopy. While ethidium homodimer-1 is cell impermeant, nuclei of fixed tissues can be stained by cell permeabilisation techniques to take advantage of the intense nuclear staining produced by this fluorescent dye. Therefore, for the ethidium

homodimer-1 and lamin B1 stain, deparaffinised sections were permeabilised and antigenicity was retrieved by microwaving in 1 mM EDTA. Non-specific staining was blocked with 10% donkey serum. The slides were incubated with a 1:670 dilution of rabbit anti-lamin B1 (product PA5-19468, Thermo Scientific, Rockford, IL) for 8 min at room temperature. The secondary antibody was Alexa 488 donkey anti-rabbit (Molecular Probes/Invitrogen, Eugene, OR). After rinsing, the slides were incubated with ethidium homodimer-1 (1  $\mu$ M) for 45 min to stain nuclei.

Lamin B1 and ethidium homodimer-1-stained sections were imaged using a Zeiss laser scanning confocal microscope (LSM 510, Carl Zeiss microscopy, Thornwood, NY). Foci with MWCNT deposition were identified using transmitted light. Ethidium homodimer-1 and lamin B1 staining were identified by fluorescence and precise localisation of MWCNT in optical sections was done using reflected light and multi-tracking with Zen 2009 software. Using the live imaging feature, serial 0.8  $\mu$ m optical sections were examined until MWCNT localisation was confirmed in the nucleus. The optical section with nuclear MWCNT was then saved as a high-resolution image.

## Statistics

All outcomes yielding quantitative values were analysed with parametric analysis of variance (ANOVA). This was performed using an unequal variance model available in SAS PROC MIXED. Ordinal measurements resulting from histopathology were analysed with non-parametric ANOVA. This was performed using the SAS procedure PROC NPAR1WAY with an exact Kruskal-Wallis test to account for ties in the data. All statistical tests in this study are two-tailed with an  $\alpha = 0.05$  significance level.

## Results

### Characterisation of Bulk MWCNT

High-resolution transmission electron microscopy (TEM) images of bulk MWCNT showed the distinctive crystalline structure of MWCNT (Figure 1). The bulk MWCNT samples were measured by XPS. The survey-scan spectrum obtained from the MWCNT sample (Figure 2A) shows that there was a dominant C 1s peak and a very small oxygen peak. No other elements were found by XPS measurements. In the detailed-scan XPS spectrum (Figure 2B) of the C 1s core level, the peak at 284.6 eV could be assigned to the sp<sup>2</sup>-bonded carbon atoms. The peaks at 285.0 and 286.2 eV indicates the presence of a small amount of –C–OH group. Trace metal contamination of aerosolized MWCNT was 1.32%, with iron (1.06%) being the major metal contaminant.

### Electron spin resonance (ESR) studies

Acellular electron spin resonance (ESR) experiments were conducted to determine if MWCNT produced reactive oxygen species (ROS). The Fenton reaction ( $\text{Fe}^{2+} + \text{H}_2\text{O}_2 \rightarrow \text{Fe}^{3+} + \cdot\text{OH} + ^-\text{OH}$ ) was used as a source of  $\cdot\text{OH}$  radicals. An aqueous solution containing  $\text{Fe}^{2+}$ ,  $\text{H}_2\text{O}_2$  and a spin trap (DMPO) in PBS (pH 7.4) generated a 1:2:2:1 quartet with hyperfine splittings of 15 G (Figure 3A). Based on these splitting constants, the 1:2:2:1 quartet was assigned to a DMPO/ $\cdot\text{OH}$  adduct as an indirect evidence for  $\cdot\text{OH}$  generation.

When DM was used as the aqueous buffer instead of PBS, the ESR signal was essentially identical to that in PBS (Figure 3B). Addition of MWCNT to the reaction mixture decreased the ESR signal, indicating that MWCNT were scavenging  $\cdot\text{OH}$  being generated from the Fenton reaction (Figure 3C). Finally, when MWCNT were substituted for  $\text{Fe}^{2+}$  in the reaction, no  $\cdot\text{OH}$  generation was detected, indicating the iron present in MWCNT was not capable of generating measurable ROS (Figure 3D), presumably because the iron is encapsulated by carbon.

### Aerosol mass concentration

Previously, we have successfully used the acoustical-based computer-controlled system to generate a stable MWCNT aerosol for animal exposures, and demonstrated that it is capable of maintaining a mean aerosol concentration to within  $0.1 \text{ mg/m}^3$  of the selected aerosol concentration target value (McKinney et al. 2009). In this study, the MWCNT aerosol mass concentration was continuously monitored with a Data RAM, and gravimetric determinations with Teflon filters were used to calibrate and verify the Data RAM readings. The mass concentration had a daily range of  $8.8\text{--}10.9 \text{ mg/m}^3$ , not including the initial rise time and fall time during the start and end of each exposure, with a mean and standard deviation of  $10.02 \pm 0.35 \text{ mg/m}^3$  throughout the study.

### Particle morphology

Particle morphology of MWCNT aerosol samples from our exposure chamber was analysed by TEM (Figure 4A) and field emission scanning electron microscopy (FESEM) (Figure 4B). The images indicated a diverse configuration of MWCNT particle shapes ranging from single fibre-like nanotubes to tangled agglomerates.

### Particle size distribution

The MOUDI cascade impactor was used to determine the mass-and number-based particle size distribution of the MWCNT aerosol in the exposure chamber. However, while the mass-based size distribution had a peak on the sixth stage of the MOUDI samples by gravimetric measurements, the number-based distribution revealed a peak on the eighth stage of the samples by visually inspecting the filters under a TEM (Figure 5). The results indicate a mass mode aerodynamic diameter of  $1.3 \mu\text{m}$  and a count mode aerodynamic diameter of  $0.42 \mu\text{m}$ . Figure 6 shows a typical size distribution of MWCNT particles collected from the chamber ( $M$  = mass concentration and  $D_{\text{ae}}$  = aerodynamic diameter). When characterised by log normal statistics, the distribution had a mass median aerodynamic diameter (MMAD) of  $1.5 \mu\text{m}$  and geometric standard deviations (GSD) of 1.67.

### MWCNT lung burden and distribution

MWCNT exposure resulted in significantly increased lung burdens at each exposure time (Figure 7). The MWCNT lung burden was linearly related to exposure duration, ranging from  $6.6 \pm 0.5$  to  $30.6 \pm 1.2 \mu\text{g/lung}$  after 2 and 12 days of exposure, respectively. The distribution of MWCNT in mice with a lung burden of  $13.0 \mu\text{g}$  (4 days exposure) was determined one day after the exposures were concluded. No MWCNT were observed in air-exposed controls (Figure 8A), whereas MWCNT were observed in the bronchioles and

proximal alveolar region of MWCNT-exposed mice (Figure 8B). Morphometric analyses determined that the airways had 24% of the total lung burden, of which 11.7% was in the airspace, 4.5% was in the tissue and 8.1% was in the macrophages (Figure 8C). The alveolar region had 76% of the total lung burden, which was distributed 14.6% in the airspace, 11.9% in the tissue and 49.2% in the macrophages (Figure 8C). Finally, MWCNT were also observed at the pleural wall (Figure 8D).

### Pulmonary inflammation and damage

MWCNT-induced pulmonary inflammation was assessed by determining WLL polymorphonuclear leukocytes (PMN) (Figure 9A). All MWCNT-exposed mice had significantly higher WLL PMN levels in comparison to the air-exposed mice. In addition, inflammation was dose dependent, i.e., mice with 23  $\mu\text{g}$  MWCNT exhibited significantly greater inflammation than mice with 7 and 13  $\mu\text{g}$  MWCNT lung burdens. Furthermore, WLL PMN levels for mice with 31  $\mu\text{g}$  MWCNT lung burdens was higher than that for mice with 23  $\mu\text{g}$  MWCNT lung burdens, although this increase was not statistically significant. The chemokine KC, which is a neutrophil chemoattractant, was determined in WLL fluid (Figure 9B). All MWCNT-exposed mice had significantly higher WLL fluid KC concentrations in comparison to corresponding air-exposed controls. In MWCNT-exposed mice, WLL fluid KC concentrations exhibited a significant increase as MWCNT lung burden increased.

MWCNT-induced cytotoxicity in the lung was assessed by determining WLL fluid LDH activities (Figure 10A). All MWCNT-exposed mice had significantly higher WLL fluid LDH activities versus corresponding air-exposed controls. LDH activities were not significantly different between mice with MWCNT lung burdens of 23 and 30  $\mu\text{g}$ , but a significant dose-dependent increase was observed for mice with lung burdens between 7 and 23  $\mu\text{g}$  MWCNT.

WLL fluid albumin concentrations were determined as a marker of the integrity of the alveolar air–blood barrier (Figure 10B). All MWCNT-exposed mice had significantly higher WLL fluid albumin concentrations in comparison to air-exposed controls. WLL fluid albumin concentrations exhibited dose-dependence for mice with lung burdens ranging from 7 to 23  $\mu\text{g}$ , but no statistically significant difference in WLL fluid albumin was present between mice with 23 and 30  $\mu\text{g}$  MWCNT lung burdens.

### Histopathology

In the lung, histopathologic alterations were principally characterised by (1) inflammation centered at the bronchioalveolar junction, (2) hyperplasia and hypertrophy of the bronchiolar epithelium, (3) airway mucous metaplasia, (4) fibrosis and (5) vascular changes (Table I). In addition, the pleura of two mice were penetrated by MWCNT.

Lung inflammation identified by histopathology was associated with deposition of MWCNT (Figures 11A, 11B). As noted above, MWCNT were most frequently deposited in bronchioles and the proximal alveolar regions. Thus, pulmonary inflammation was centred near the bronchioalveolar junction. At all time points, the principal inflammatory cells were consistently macrophages and neutrophils. Giant cells were first observed at the 8-day

exposure time point and were an occasional component of the inflammatory response in five of six MWCNT-exposed mice at the 8-day time point and six of six MWCNT-exposed mice at the 12-day time point. Giant cells were not seen in the lungs of control mice. One MWCNT-exposed mouse at the 12-day time point had multifocal moderate eosinophilic crystalline pneumonia, a condition associated with spontaneous or treatment-associated accumulations of YM1 protein in mice (Hoenerhoff et al. 2006).

MWCNT-induced cytopathology was observed in lung macrophages. Those changes included penetration of the cytoplasmic and nuclear membrane. Focal nuclear rarefaction and/or chromatin condensation was sometimes observed in association with penetration of the nuclear membrane. In addition, some macrophages containing MWCNT had no visible nucleus or decreased nuclear staining consistent with karyolysis. One dividing macrophage had MWCNT incorporated into an abnormal mitotic figure (Figure 11C), a change reminiscent of those previously reported after exposure to single-walled carbon nanotubes (Sargent et al. 2012; Shvedova et al. 2008). Confocal microscopy of lamin B1 and ethidium homodimer-1 stained sections as well as enhanced-darkfield light microscopic imaging confirmed penetration of rare nuclei by MWCNTs (Figures 12A, B and C).

Bronchiolar epithelial cell hypertrophy and hyperplasia were present in all MWCNT-exposed mice at all time points (Table I, Figure 11B). Mitotic figures in the airway epithelium, while rare, were seen in all MWCNT-exposed mice at the 4-day time point and thereafter were observed in only one mouse in the 12-day MWCNT exposure group. Rare intraepithelial MWCNT were seen in seven of eight mice after 4 days of MWCNT exposure and two of six mice after 8 days of MWCNT exposure (Figure 11D). Intraepithelial MWCNT were not seen in mice exposed to MWCNT for 12 days.

Mucous metaplasia of airway epithelial cells was observed in seven of eight MWCNT-exposed mice at the 4-day exposure time point. At the 8- and 12-day time points, mucous metaplasia was observed in all MWCNT-exposed (Table I, Figure 11E).

Lung fibrosis was generally minimal to mild in severity, principally bronchiolocentric and was associated with sites of inflammation in the lungs of all MWCNT-exposed mice at the 8- and 12-day time points. In addition to being associated with inflammation, fibrosis was associated with an expanded interstitium and the presence of interstitial MWCNT (Figure 11F).

Vascular changes were consistently observed in the lungs of MWCNT-exposed mice although affected vessels were rare within each section. The features of vascular changes varied and include medial hypertrophy and contraction, mural neutrophil infiltrates and rare mural MWCNT (Table I, Figure 11G).

Pleural penetration was seen in two mice, both from the 12-day time point. In one of these mice, MWCNT extended from the pleura into a macrophage on the pleural surface (Figure 11H). Pleural penetration was confirmed using enhanced darkfield light microscopy (Figure 12D).

In the tracheobronchial lymph nodes, histopathologic alterations were principally characterised by (1) translocation of MWCNT and (2) expansion of the deep paracortex. Tracheobronchial lymph nodes of the mouse are extremely small, but adequate samples for histopathologic evaluations were available for four of eight control mice and seven of eight MWCNT-exposed mice at the 4-day time point, four of six control mice and two of six MWCNT-exposed mice at the 8-day time point, and three of six control mice and five of six MWCNT-exposed mice at the 12-day time point. MWCNT were identified in lymph nodes of five MWCNT-exposed lymph nodes after 4 days of exposure and in all MWCNT-exposed mice after 8 and 12 days of exposure. The MWCNT in the lymph node were predominantly localised to deep paracortical region that was expanded in three of seven MWCNT-exposed lymph nodes after a 4-day exposure and in all MWCNT-exposed lymph nodes after 8 or 12 days of exposure (Table II, Figure 13). In the paracortex, cells containing MWCNT were morphologically consistent with macrophages and dendritic cells. Cells containing both MWCNT and apoptotic debris were also observed. Cytopathology changes include penetration of the nuclear membrane with associated nuclear rarefaction and/or chromatin condensation (Figure 14).

In the nose, the principal histopathologic alteration after the 12-day exposure was neutrophilic inflammation (Table III). Neutrophilic inflammation was present in level T1 in five of six MWCNT-exposed mice. In level T2 and level T3, neutrophilic inflammation was present in all MWCNT-exposed mice. In level T4, neutrophilic inflammation was present in four of six MWCNT-exposed mice. In addition, intraepithelial hyaline droplets were seen in the respiratory epithelium of the nose of all MWCNT-exposed mice and affected levels T2 (five of six mice), T3 (six of six mice) and T4 (six of six mice). MWCNT were seen in nasal sections from four mice. In two mice, intraepithelial MWCNT were observed and MWCNT were seen in the mucous layer of four mice.

## Discussion

The primary objective of this investigation was to evaluate MWCNT-induced pulmonary inflammation, damage and fibrosis 1 day post-exposure to an aerosol of MWCNT. To accomplish this, mice were exposed to aerosolized MWCNT (10 mg/m<sup>3</sup>, 5 h/day) for either 2, 4, 8 or 12 days. At 1 day post-exposure, MWCNT lung burdens ranged from 7 µg (2 days exposure) to 31 µg (12 days exposure). In order to evaluate the relationship of these MWCNT lung burdens to human MWCNT exposures, we determined if the MWCNT lung burdens in these mice are relevant human occupational exposures.

Data on human exposures to MWCNT are limited in number and in regards to the exact levels of MWCNT in the airborne samples. The first study reported workplace MWCNT-containing airborne dust levels of approximately 400 µg/m<sup>3</sup> in a research laboratory (Han et al. 2008), while a later study reported a peak total particle concentration of 320 µg/m<sup>3</sup> with a mean of 106 µg/m<sup>3</sup> based on results obtained from monitoring total workplace dust levels at seven MWCNT facilities (Lee et al. 2010). However, both studies may have overestimated MWCNT exposure because the MWCNT structures observed in the research laboratory varied between agglomerates to individual fibres, and not all of the particles were MWCNT (Han et al. 2008), while samples from the seven MWCNT facilities included significant

amounts of metal nanoparticles used as catalyst for MWCNT production (Lee et al. 2010). However limited these workplace exposure studies may be, they currently are the only ones available to evaluate if the MWCNT lung burdens measured in this study are relevant to human occupational exposures.

Assuming a mouse alveolar epithelium surface area of  $0.05 \text{ m}^2$  (Stone et al. 1992), the  $7 \text{ }\mu\text{g}$  MWCNT lung burden would result in  $140 \text{ }\mu\text{g MWCNT/m}^2$  alveolar epithelium, whereas the  $31 \text{ }\mu\text{g}$  MWCNT lung burden would result in  $620 \text{ }\mu\text{g MWCNT/m}^2$  alveolar epithelium. Using the MWCNT MMAD =  $1.5 \text{ }\mu\text{m}$ , minute ventilation of  $20 \text{ L/min}$  for a person performing light work (Galer et al. 1992), deposition fraction of 30% (Phalen 1984) and human alveolar epithelium surface area of  $102 \text{ m}^2$  (Stone et al. 1992), approximate human lung burden per month for a workplace MWCNT exposure of 106 or  $400 \text{ }\mu\text{g/m}^3$  (Han et al. 2008; Lee et al. 2010) would be 60 and  $226 \text{ }\mu\text{g MWCNT/m}^2$  alveolar epithelium, respectively. Thus,  $17 \text{ }\mu\text{g}$  MWCNT lung burden in mouse approximates human deposition for a person performing light work for 2.5 – 5 months, while the  $77 \text{ }\mu\text{g}$  MWCNT lung burden in mice approximates human deposition for a person performing light work for 8 – 25 months. As previously stated, the two studies which have reported human MWCNT exposures likely have overestimated MWCNT exposure levels. If we assume actual human average, daily MWCNT aerosol exposure may be 10 times lower ( $10\text{--}40 \text{ }\mu\text{g/m}^3$  MWCNT) than estimates based on total airborne dust levels of 106 and  $400 \text{ }\mu\text{g/m}^3$  (Han et al. 2008; Lee et al. 2010), the  $31 \text{ }\mu\text{g}$  MWCNT lung burden in mouse would approximate human deposition for a person performing light work for approximately 27-103 months, i.e., 2.3–8.5 years. Thus, these estimates suggest that the mouse MWCNT lung burdens in this study approximate feasible human occupational exposures.

A panel of experts has recommended the characterisation of both “as-produced” and “as-administered” nanoparticles used in toxicological studies (Oberdorster et al. 2005), and later it was suggested that nanotoxicology studies that lack adequate nanoparticle characterisation may not provide meaningful data or conclusions (Warheit 2008). Although the manufacturer of MWCNT used in these studies was the same as in our earlier study (Porter et al. 2010), it was necessary to use a different lot of MWCNT for the present study. Because lot-to-lot variation is a potential confounding factor in interpreting the results, using the guidance from experts in nanotoxicology (Oberdorster et al. 2005; Warheit 2008), we invested significant effort into the characterisation of the MWCNT used in this study so that the results could be compared to our previous *in vivo* study (Porter et al. 2010) as well as data reported by others.

The bulk sample of MWCNT was analysed using several different techniques: (1) high-resolution TEM, (2) XPS and (3) ESR spectroscopy. High-resolution TEM determined that the nanoparticles used in this study were MWCNT, and not some other form of carbonaceous material. XPS analyses determined a C 1s peak at  $284.6 \text{ eV}$ , which corresponds to the  $\text{sp}^2$ -hybridised graphite-like carbon atoms (Ago et al. 1999; Chen et al. 1999). The C 1s peak at  $285 \text{ eV}$  is attributed to the  $\text{sp}^3$ -hybridised carbon atoms with disordered structure (Pinault et al. 2005), whereas the C 1s peak component at  $286.2 \text{ eV}$  is attributed to C–O bonds (Felten et al. 2006; Stankovich et al. 2006). The later observation indicates the formation of the hydroxyl groups on the MWCNT surface (Felten et al. 2006).

The XPS analyses of the MWCNT used in this study were very similar to those reported by our laboratory using a different lot of MWCNT from the same manufacturer (Porter et al. 2010). Aerosol samples of the MWCNT were collected and analysed for 31 different metals because metals are used as catalysts for MWCNT synthesis and can remain as contaminants post-production in MWCNT. The metal analyses determined the total metal content was relatively low, 1.32%, with iron (1.06%) being the major contaminant.

Intracellular ROS production after exposure to SWCNT or MWCNT has been demonstrated with NR8383 and A549 cells, an observation which suggests that exposure to CNT induces cellular oxidative stress (Pulskamp et al. 2007). Acid treatment of the CNT used in that study prior to exposure resulted in reduction of CNT-induced cellular oxidative stress, which led to the suggestion that metal contaminants in the CNT samples, and not the CNTs themselves, were responsible for the cellular oxidative stress response (Pulskamp et al. 2007). However, we had to at least consider the possibility that the MWCNT in this study may induce oxidant production despite the low metal contamination of the MWCNT used in the present study. Cell-free ESR experiments determined that MWCNT did not generate ROS. These findings are consistent with previous studies, which also determined that cell-free aqueous suspensions of MWCNT do not generate ROS (Fenoglio et al. 2006; Porter et al. 2010). It should also be noted that the MWCNT scavenged ROS to a small degree, which is similar to earlier findings using MWCNT from a different manufacturer (Fenoglio et al. 2006) and from our laboratory using a different lot of MWCNT from the same manufacturer (Porter et al. 2010).

The system used to generate MWCNT aerosols in this study has been previously described in detail (McKinney et al. 2009). Gravimetric determinations indicated the MWCNT mean mass concentration per exposure was  $10.02 \pm 0.35 \text{ mg/m}^3$  (mean  $\pm$  SD). The mass- and number-based particle size distribution of the MWCNT aerosol in the exposure chamber was examined using a MOUDI cascade impactor. These analyses determined a mass mode aerodynamic diameter of  $1.3 \mu\text{m}$  and a count mode aerodynamic diameter of  $0.42 \mu\text{m}$ . The distribution had a MMAD of  $1.5 \mu\text{m}$  and a GSD of 1.67. MWCNT morphology, analysed by TEM and SEM, found a diversity of particle shapes and configurations. Most importantly, these images are similar to those published in a recent report in which samples were collected from the breathing zones in a MWCNT manufacturing workplace (Han et al. 2008). This indicates that the particle size and shape of these workplace samples appear to be very similar to the samples collected in our exposure chamber, thus demonstrating that our aerosol generation system produced MWCNT aerosols representative of those occurring in a workplace. In addition, there is a striking similarity between aerosolized MWCNT structures generated in the present study and structures in the dispersed suspension of MWCNT used in a previous pharyngeal aspiration study by our laboratory (Porter et al. 2010).

The lung burdens in this inhalation study, which ranged from 7 to  $31 \mu\text{g}$  MWCNT, were similar to the doses used in our previous MWCNT aspiration study of  $10\text{--}40 \mu\text{g}$  (Porter et al. 2010). The distribution of MWCNT in mice with a lung burden of  $13.0 \mu\text{g}$  (4 days exposure) was assessed and indicated that MWCNT were deposited in both the alveolar and airway regions of the lung. The largest deposition was in the AM in the alveolar region, suggesting

that the inhaled MWCNT were being phagocytised and the process of clearance from the lung had been initiated. The MWCNT in the airways may have resulted from direct deposition from the aerosol, as well as AM moving up the mucociliary escalator as part of the clearance process. In addition, our laboratory has previously reported that after pharyngeal aspiration of MWCNT, MWCNT penetrated the pleura (Porter et al. 2010; Mercer et al. 2010). Lastly, our laboratory has previously reported that 56 days after pharyngeal aspiration to MWCNT that inflammation had extended to the pleura, and MWCNT had penetrated the pleura. Here we report similar data obtained from mice one day after completion of a 4-day aerosol exposure to MWCNT, i.e., two mice had pleural penetration after 12 days of MWCNT inhalation. This result adds further weight to the hypothesis that MWCNT, if persistent in the lung, could cause diseases that are reminiscent of the classic inhalable occupational fibre: asbestos (Donaldson et al. 2006; Donaldson & Tran 2004).

MWCNT-induced pulmonary inflammation was assessed by determining WLL PMNs, and indicated significant inflammation was induced by exposures of varying durations and lung burdens. Furthermore, MWCNT-induced pulmonary inflammation in WLL was biphasic, i.e., inflammation induced by MWCNT lung burdens of 7 and 13  $\mu\text{g}$  was similar, while that induced by MWCNT lung burdens of 23 and 31  $\mu\text{g}$  increased further. This biphasic response may be due to an increase in lung neutrophil chemoattractant KC, which increased with increasing MWCNT lung burden. Thus, it appears that pulmonary neutrophilic inflammation is caused by both MWCNT deposition as well as the expression of inflammatory mediators, such as KC. Semi-quantitative histopathology assessment of lung inflammation is a less quantitative measure than WLL but confirmed the presence of persistent inflammation in the lung, involvement of the pulmonary interstitium and the development of fibrosis in some foci of interstitial inflammation. In addition, airway mucous metaplasia was demonstrated in histologic sections. Since mucous metaplasia is a known response of airway epithelial cells to a variety of cytokines, this change was consistent with the persistent inflammation demonstrated by histopathology and WLL.

It was expected that MWCNT exposure might also result in some cytotoxic damage in the lung. To measure this, MWCNT-induced cytotoxicity, measured by WLL fluid LDH, and permeability of the alveolar air–blood barrier, as measured by WLL fluid albumin, was determined, respectively. In contrast to the biphasic nature of the lung inflammatory response, these parameters of toxicity had a nearly linear response to MWCNT lung burden. This suggests that these parameters of lung toxicity are being influenced most directly by the amount of MWCNT deposited in the lung. Another occupationally important dust, silica, induces cytotoxic damage to the lung via particle-induced ROS generation (Vallyathan et al. 1995) and/or cellular-mediated ROS generation (Blackford et al. 1994). The ESR studies reported here determined MWCNT do not generate ROS, making it unlikely that the cytotoxic damage resulted from direct MWCNT-mediated ROS. However, MWCNT-induced cellular-mediated ROS production has been reported (Pulskamp et al. 2007), and this may contribute to the observed cytotoxicity. The presence of airway mucous metaplasia in the MWCNT-exposed mice in our study is consistent with the presence of cell-mediated cytotoxic damage, because mucous metaplasia can be a response to a variety of cytokines (Young et al. 2007; Lai & Rogers 2010). Furthermore, the interaction of MWCNT with the

alveolar epithelial cells noted in the FESEM images and histopathology sections may also impact both LDH release and increased permeability of the alveolar air–blood barrier.

A previous MWCNT inhalation study exposed mice to aerosols of either 1 or 30 mg/m<sup>3</sup> MWCNT for 6 h (Ryman-Rasmussen et al. 2009b). The calculated dose for the mice exposed to 30 mg/m<sup>3</sup> MWCNT for 6 h falls within the range of MWCNT lung burdens determined in the present study. Data presented in the Ryman-Ramussen et al. study indicated that inhaled MWCNT were contained in macrophages; these macrophages migrated to the subpleural region and significant subplueral fibrosis was observed. Furthermore, the authors speculated the activated macrophages containing MWCNT travel through the pleural lymphatics. Micron-sized particles have been demonstrated to move from the alveolar region of the lung to the draining lymph nodes within macrophages and neutrophils (Harmsen et al. 1987; Harmsen et al. 1985). Small spherical nanoparticles less than 34 nm in diameter can be transported from the alveolar region to the draining lymph nodes within minutes of administration suggesting that the lymphatic transport of the smallest nanoparticles may not require phagocytosis (Choi et al. 2010). Indeed, it has previously been noted that many nanomaterials are preferentially transported in the lymphatics (Riviere 2009). In the present study, we demonstrated intracellular MWCNT on the surface of the pleura (Figure 11H) and multiple MWCNT in lymph nodes (Figure 14), observations supporting the hypothesis that activated macrophages containing MWCNT travel through the lymphatics and reach the pleura.

Translocation of MWCNT from the lung to the tracheobronchial lymph node has previously been demonstrated in rats (Aiso et al. 2011). Increased paracortical cellularity has also been previously noted in the lymph nodes of rats inhaling MWCNT (Pauluhn 2010). Decreased T-cell-dependent immunologic responses have previously been observed in mice inhaling MWCNT (Mitchell et al. 2007), a response that has been proposed to be mediated predominantly via transforming growth factor- $\beta$  release from MWCNT-exposed lungs (Mitchell et al. 2009). In the present study, we identified translocation of MWCNT from the lung to the tracheobronchial lymph nodes in the mouse. Translocation of MWCNT to the lymph nodes was accompanied by lymph node enlargement with hyperplasia principally in the deep paracortical units of the lymph node. Thus, our study confirms that in the mouse as well as the rat, the draining lymph nodes are a site for MWCNT clearance from the lung and that the lymph node responds to the presence of the translocated MWCNT by hyperplasia. The deep paracortical units of the lymph node are preferentially occupied by dendritic cells and T-lymphocytes, and are sites of interaction between antigen-presenting cells and T-lymphocytes (Willard-Mack 2006), suggesting that MWCNT translocation to the deep paracortical units of the lymph node we observed in our study may alter T-cell responses, either locally or through release of mediators.

A long-standing issue in pulmonary toxicology is the relevance of bolus exposure to particles by intratracheal instillation or pharyngeal aspiration to pulmonary responses resulting from inhalation exposure (Henderson et al. 1995). The results of the present short-term MWCNT inhalation study afford a unique opportunity to address this issue, since the MWCNT pharyngeal aspiration study previously reported by our laboratory (Porter et al. 2010) used similar material at nearly equivalent lung burdens, and measured the same end

points over the same post-exposure time. Additionally, the structure sizes generated by aerosolization of dry MWCNT in the present study were strikingly similar to those obtained when MWCNT were suspended in dispersion medium (Porter et al. 2008), which represents a diluted artificial alveolar lining fluid. Since the MWCNT used and the experimental design of the present inhalation study and our previous aspiration study when MWCNT were suspended in dispersion medium (Porter et al. 2010) are similar, one can compare the inflammatory and damage responses at a given lung burden 1 day after exposure. As shown in Figure 15, the degree of infiltration of PMNs into the airspaces after aspiration does not significantly differ from the inflammatory response after inhalation of MWCNT.

It has also been argued that inhalation exposure results in a more even distribution of particles throughout the lung, while bolus exposure creates deposition hot spots (Henderson et al. 1995). However, mice exposed to fluorescent beads by pharyngeal aspiration exhibited a relatively uniform distribution of particles throughout the various lung lobes (Rao et al. 2003). Morphometric analysis of MWCNT distribution after pharyngeal aspiration from a study conducted by our laboratory (Porter et al. 2010) reported that 1 day after aspiration, 18% of MWCNT structures were in the airways, while 81% were in the alveolar region of the lung (Mercer et al. 2010). Morphometric data in the present study found very similar results indicating that 1 day after inhalation of MWCNT 24% of structures were in the airways, while 76% were in the alveolar region. Additionally, MWCNT were found to reach the subpleural tissue after both inhalation (present study) and pharyngeal aspiration (Mercer et al. 2010; Porter et al. 2010). Therefore, aspiration of a well-dispersed suspension of MWCNT appears to result in a pulmonary distribution which models closely that seen after inhalation of a similar lung burden of MWCNT.

Finally, NIOSH (NIOSH 2010) conducted a risk analysis to compare benchmark human exposure concentration for MWCNT using data from a mouse aspiration study (Porter et al. 2010) versus a 3-month inhalation study (Ma-Hock et al. 2009). Benchmark exposure concentration for MWCNT-induced pulmonary fibrosis or granulomatous inflammation was  $0.61 \mu\text{g}/\text{m}^3$  for the aspiration versus  $0.5 \mu\text{g}/\text{m}^3$  for the inhalation study, respectively. Therefore, evidence indicates that when CNT samples of similar dispersion are used, aspiration studies can predict a pulmonary response that is consistent with short-term inhalation studies when dosed at an equal mass lung burden.

In summary, the data reported here indicate that the lung burdens of MWCNT in this study represent lung burdens relevant to estimated human occupational exposures and caused dose-dependent pulmonary inflammation and damage, as assessed by WLL and histopathological methods. MWCNT exposure also caused rapid development of pulmonary fibrosis. Furthermore, the data demonstrate that MWCNT can reach and penetrate the pleura after aerosol exposure, confirming earlier findings by our laboratory (Porter et al. 2010; Mercer et al. 2010) that this occurred after pharyngeal aspiration exposure to MWCNT. However, the possible development of adverse health outcomes resulting from MWCNT reaching, and in some cases penetrating, the lung pleura still requires further investigation.

## Acknowledgments

The authors would like to thank Hodogaya Chemical Company for the generous donation of the MWCNT used in this study. The authors would like to thank Ming Li and Min-gjiaZhi at West Virginia University for assistance with the XPS measurements. The technical expertise and assistance of Kara Fluharty and Sherri Friend in immunofluorescence and confocal microscopy are gratefully acknowledged.

## References

- Ago H, Kugler T, Cacialli F, Salaneck WR, Shaffer MSP, Windle AH, et al. Work functions and surface functional groups of multiwall carbon nanotubes. *J Phys Chem B*. 1999; 103:8116–8121.
- Aiso S, Kubota H, Umeda Y, Kasai T, Takaya M, Yamazaki K, et al. Translocation of intratracheally instilled multiwall carbon nanotubes to lung-associated lymph nodes in rats. *Ind Health*. 2011; 49:215–220. [PubMed: 21173528]
- American Registry of Pathology. Manual of histologic staining methods of the armed forces institute of pathology. New York: McGraw-Hill; 1968.
- Blackford JA, Antonini JM, Castranova V, Dey RD. Intratracheal instillation of silica up-regulates inducible nitric-oxide synthase gene-expression and increases nitric-oxide production in alveolar macrophages and neutrophils. *Am J Respir Cell Mol Biol*. 1994; 11:426–431. [PubMed: 7522485]
- Chen P, Wu X, Sun X, Lin J, Ji W, Tan KL. Electronic structure and optical limiting behavior of carbon nanotubes. *Phys Rev Lett*. 1999; 82:2548–2551.
- Choi HS, Ashitate Y, Lee JH, Kim SH, Matsui A, Insin N, et al. Rapid translocation of nanoparticles from the lung airspaces to the body. *Nat Biotechnol*. 2010; 28:1300–1303. [PubMed: 21057497]
- Donaldson K, Aitken R, Tran L, Stone V, Duffin R, Forrest G, et al. Carbon nanotubes: a review of their properties in relation to pulmonary toxicology and workplace safety. *Toxicol Sci*. 2006; 92:5–22. [PubMed: 16484287]
- Donaldson K, Tran CL. An introduction to the short-term toxicology of respirable industrial fibres. *Mutat Res*. 2004; 553:5–9. [PubMed: 15288528]
- Elder A, Gelein R, Finkelstein JN, Driscoll KE, Harkema J, Oberdorster G. Effects of subchronically inhaled carbon black in three species. I. Retention kinetics, lung inflammation, and histopathology. *Toxicol Sci*. 2005; 88:614–629. [PubMed: 16177241]
- Felten A, Bittencourt C, Pireaux JJ. Gold clusters on oxygen plasma functionalized carbon nanotubes: XPS and TEM studies. *Nanotechnology*. 2006; 17:1954–1959.
- Fenoglio I, Tomatis M, Lison D, Muller J, Fonseca A, Nagy JB, et al. Reactivity of carbon nanotubes: free radical generation or scavenging activity? *Free Radic Biol Med*. 2006; 40:1227–1233. [PubMed: 16545691]
- Galer DM, Leung HW, Sussman RG, Trzos RJ. Scientific and practical considerations for the development of occupational exposure limits (Oels) for chemical-substances. *Regul Toxicol Pharmacol*. 1992; 15:291–306. [PubMed: 1509122]
- Han JH, Lee EJ, Lee JH, So KP, Lee YH, Bae GN, et al. Monitoring multiwalled carbon nanotube exposure in carbon nanotube research facility. *Inhal Toxicol*. 2008; 20:741–749. [PubMed: 18569096]
- Harmsen AG, Mason MJ, Muggenburg BA, Gillett NA, Jarpe MA, Bice DE. Migration of neutrophils from lung to tracheobronchial lymph node. *J Leukoc Biol*. 1987; 41:95–103. [PubMed: 3468196]
- Harmsen AG, Muggenburg BA, Snipes MB, Bice DE. The role of macrophages in particle translocation from lungs to lymph nodes. *Science*. 1985; 230(4731):1277–1280. [PubMed: 4071052]
- Henderson RF, Driscoll KE, Harkema JR, Lindenschmidt RC, Chang IY, Maples KR, et al. A comparison of the inflammatory response of the lung to inhaled versus instilled particulates in F344 rats. *Fundam Appl Toxicol*. 1995; 24:183–197. [PubMed: 7737430]
- Herbert, RA.; Leininger, JR. Nose, larynx and trachea. In: Maronpot, RR.; Boorman, GA.; Gaul, BW., editors. Pathology of the mouse. Vienna, IL: Cache River Press; 1999.
- Hoenerhoff MJ, Starost MF, Ward JM. Eosinophilic crystalline pneumonia as a major cause of death in 129S4/SvJae mice. *Vet Pathol*. 2006; 43:682–688. [PubMed: 16966445]

- Hubbs AF, Goldsmith WT, Kashon ML, Frazer D, Mercer RR, Battelli LA, et al. Respiratory toxicologic pathology of inhaled diacetyl in sprague-dawley rats. *Toxicol Pathol.* 2008; 36:330–344. [PubMed: 18474946]
- Kim YA, Hayashi T, Endo M, Kaburagi Y, Tsukada T, Shan J, et al. Synthesis and structural characterization of thin multi-walled carbon nanotubes with a partially faceted cross section by a floating reactant method. *Carbon.* 2005; 43:2243–2250.
- Lai HY, Rogers DF. Mucus hypersecretion in asthma: intracellular signalling pathways as targets for pharmacotherapy. *Curr Opin Allergy Clin Immunol.* 2010; 10(1):67–76. [PubMed: 19907312]
- Lee JH, Lee S-B, Bae GN, Jeon KS, Yoon JU, Ji JH, et al. Exposure assessment of carbon nanotube manufacturing workplaces. *Inhal Toxicol.* 2010; 22:369–381. [PubMed: 20121582]
- Li J-G, Li W-X, Xu J-Y, Cai X-Q, Liu R-L, Li Y-J, et al. Comparative study of pathological lesions induced by multiwalled carbon nanotubes in lungs of mice by intratracheal instillation and inhalation. *Environ Toxicol.* 2007; 22:415–421. [PubMed: 17607736]
- Ma-Hock L, Treumann S, Strauss V, Brill S, Luizi F, Mertler M, et al. Inhalation toxicity of multiwall carbon nanotubes in rats exposed for 3 months. *Toxicol Sci.* 2009; 112:468–481. [PubMed: 19584127]
- McKinney W, Chen B, Frazer D. Computer controlled multi-walled carbon nanotube inhalation exposure system. *Inhal Toxicol.* 2009; 21:1053–1061. [PubMed: 19555230]
- Mercer RR, Hubbs AF, Scabilloni JF, Wang LY, Battelli LA, Friend S, et al. Pulmonary fibrotic response to aspiration of multi-walled carbon nanotubes. *Part Fibre Toxicol.* 2011; 8:21. [PubMed: 21781304]
- Mercer RR, Hubbs AF, Scabilloni JF, Wang LY, Battelli LA, Schwegler-Berry D, et al. Distribution and persistence of pleural penetrations by multi-walled carbon nanotubes. *Part Fibre Toxicol.* 2010; 7:28. [PubMed: 20920331]
- Mitchell LA, Gao J, Wal RV, Gigliotti A, Burchiel SW, McDonald JD. Pulmonary and systemic immune response to inhaled multiwalled carbon nanotubes. *Toxicol Sci.* 2007; 100:203–214. [PubMed: 17660506]
- Mitchell LA, Lauer FT, Burchiel SW, McDonald JD. Mechanisms for how inhaled multiwalled carbon nanotubes suppress systemic immune function in mice. *Nat Nanotechnol.* 2009; 4:451–456. [PubMed: 19581899]
- NIOSH. Method 7300. Elements by ICP (Nitric/Perchloric Acid Ashing). In: Eller, PM.; Cassinelli, ME., editors. NIOSH manual of analytical methods. Cincinnati, Ohio: U.S. Department of Health and Human Services; 1994.
- NIOSH. [Accessed on 12 July 2012] NIOSH Current Intelligence Bulletin Occupational Exposure to Carbon Nanotubes and Nanofibers. 2010. [http://www.cdc.gov/niosh/docket/review/docket161A/pdfs/carbonNanotubeCIB\\_PublicReviewOfDraft.pdf](http://www.cdc.gov/niosh/docket/review/docket161A/pdfs/carbonNanotubeCIB_PublicReviewOfDraft.pdf)
- Oberdorster G, Maynard A, Donaldson K, Castranova V, Fitzpatrick J, Ausman K. Ilsi Research Foundation/Risk Science Institute Nanomaterial Toxicity, and Group Screening Working. Principles for characterizing the potential human health effects from exposure to nanomaterials: elements of a screening strategy. *Part Fibre Toxicol.* 2005; 2:8. [PubMed: 16209704]
- Pacurari M, Qian Y, Porter DW, Wolfarth M, Wan Y, Luo D, et al. Multi-walled carbon nanotube-induced gene expression in the mouse lung: association with lung pathology. *Toxicol Appl Pharmacol.* 2011; 255:18–31. [PubMed: 21624382]
- Pauluhn J. Subchronic 13-week inhalation exposure of rats to multiwalled carbon nanotubes: toxic effects are determined by density of agglomerate structures, not fibrillar structures. *Toxicol Sci.* 2010; 113:226–242. [PubMed: 19822600]
- Phalen, RF. Inhalation studies: foundations and techniques. Boca Raton: CRC Press; 1984. Basic morphology and physiology of the respiratory tract.
- Pinaut M, Mayne-L'Hermite M, Reynaud C, Pichot V, Launois P, Ballutaud D. Growth of multiwalled carbon nanotubes during the initial stages of aerosol-assisted CCVD. *Carbon.* 2005; 43:2968–2976.
- Porter D, Sriram K, Wolfarth M, Jefferson A, Schwegler-Berry D, Andrew M, et al. A biocompatible medium for nanoparticle dispersion. *Nanotoxicology.* 2008; 2:144–154.

- Porter DW, Hubbs AF, Mercer RR, Wu NQ, Wolfarth MG, Sriram K, et al. Mouse pulmonary dose- and time course-responses induced by exposure to multi-walled carbon nanotubes. *Toxicology*. 2010; 269:136–147. [PubMed: 19857541]
- Pulskamp K, Diabate S, Krug HF. Carbon nanotubes show no sign of acute toxicity but induce intracellular reactive oxygen species in dependence on contaminants. *Toxicol Lett*. 2007; 168:58–74. [PubMed: 17141434]
- Rao GVS, Tinkle S, Weissman DN, Antonini JM, Kashon ML, Salmen R, et al. Efficacy of a technique for exposing the mouse lung to particles aspirated from the pharynx. *J Toxicol Environ Health A*. 2003; 66:1441–1452. [PubMed: 12857634]
- Riviere JE. Pharmacokinetics of nanomaterials: an overview of carbon nanotubes, fullerenes and quantum dots. *Wiley Interdiscip Rev Nanomed Nanobiotechnol*. 2009; 1:26–34. [PubMed: 20049776]
- Ryman-Rasmussen JP, Cesta MF, Brody AR, Shipley-Phillips JK, Everitt JJ, Tewksbury EW, et al. Inhaled carbon nanotubes reach the subpleural tissue in mice. *Nat Nanotechnol*. 2009a; 4:747–751. [PubMed: 19893520]
- Ryman-Rasmussen JP, Tewksbury EW, Moss OR, Cesta MF, Wong BA, Bonner JC. Inhaled multiwalled carbon nanotubes potentiate airway fibrosis in murine allergic asthma. *Am J Respir Cell Mol Biol*. 2009b; 40:349–358. [PubMed: 18787175]
- Sargent LM, Hubbs AF, Young SH, Kashon ML, Dinu CZ, Salisbury JL, et al. Single-walled carbon nanotube-induced mitotic disruption. *Mutat Res*. 2012; 745:28–37. [PubMed: 22178868]
- Shvedova AA, Kisin E, Murray AR, Johnson VJ, Gorelik O, Arepalli S, et al. Inhalation vs. aspiration of single-walled carbon nanotubes in C57BL/6 mice: inflammation, fibrosis, oxidative stress, and mutagenesis. *Am J Physiol Lung Cell Mol Physiol*. 2008; 295:L552–L565. [PubMed: 18658273]
- Stankovich S, Piner RD, Chen XQ, Wu NQ, Nguyen ST, Ruoff RS. Stable aqueous dispersions of graphitic nanoplatelets via the reduction of exfoliated graphite oxide in the presence of poly (sodium 4-styrenesulfonate). *J Mater Chem*. 2006; 16:155–158.
- Stone KC, Mercer RR, Gehr P, Stockstill B, Crapo JD. Allometric relationships of cell numbers and size in the mammalian lung. *Am J Respir Cell Mol Biol*. 1992; 6:235–243. [PubMed: 1540387]
- Vallyathan V, Castranova V, Pack D, Leonard S, Shumaker J, Hubbs AF, et al. Freshly fractured quartz inhalation leads to enhanced lung injury and inflammation – potential role of free-radicals. *Am J Respir Crit Care Med*. 1995; 152:1003–1009. [PubMed: 7663775]
- Warheit DB. How meaningful are the results of nanotoxicity studies in the absence of adequate material characterization? *Toxicol Sci*. 2008; 101:183–185. [PubMed: 18300382]
- Willard-Mack CL. Normal structure, function, and histology of lymph nodes. *Toxicol Pathol*. 2006; 34:409–424. [PubMed: 17067937]
- Young HW, Williams OW, Chandra D, Bellinghausen LK, Perez G, Suarez A, et al. Central role of Muc5ac expression in mucous metaplasia and its regulation by conserved 5' elements. *Am J Respir Cell Mol Biol*. 2007; 37:273–290. [PubMed: 17463395]
- Young JT. Histopathologic examination of the rat nasal cavity. *Fundam Appl Toxicol*. 1981; 1:309–312. [PubMed: 6764423]

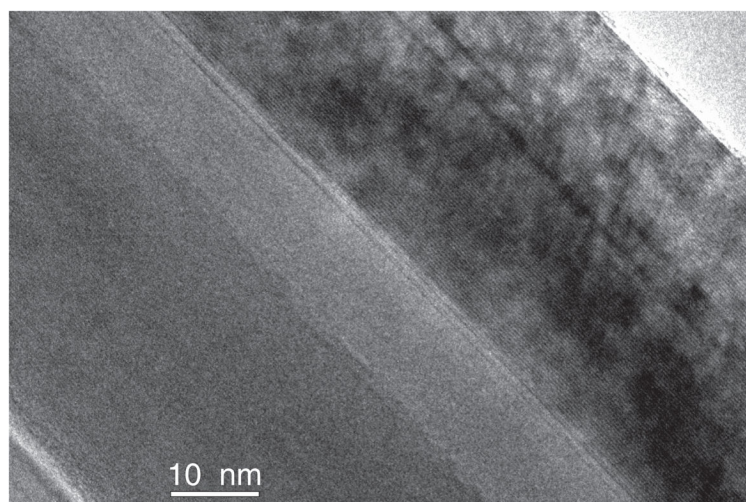


**Figure 1.** High-resolution transmission electron micrograph of MWCNT. A representative high-resolution transmission electron micrograph of the bulk MWCNT sample shows the distinctive crystalline structure of MWCNT.

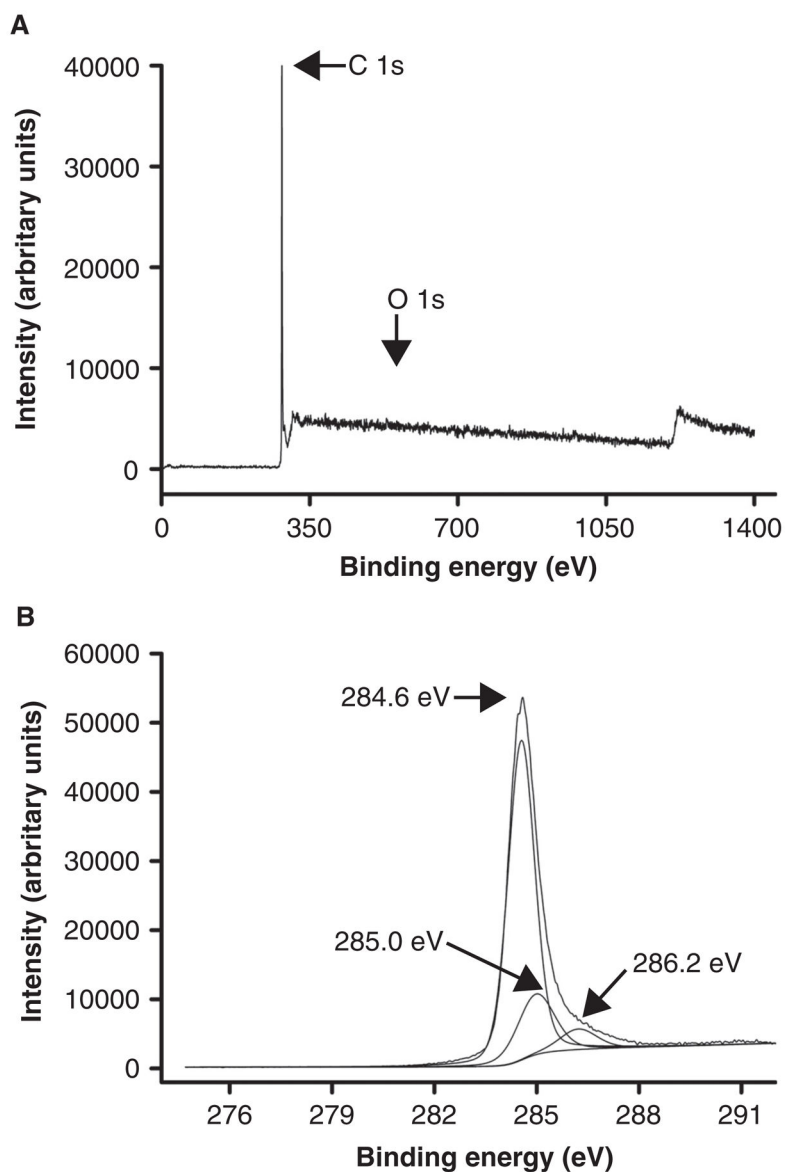


**Figure 2.**

XPS spectra of MWCNT. (Panel A) XPS survey-scan spectrum has a dominant carbon (C 1s) peak and a small oxygen (O 1s) peak. (Panel B) The detailed-scan XPS spectrum of the C 1s core level determined a C 1s peak at 284.6 and 285 eV, which corresponds to the sp<sup>2</sup>-hybridised graphite-like carbon atoms of the carbon nanotube and the sp<sup>3</sup>-hybridised carbon atoms with disordered structure, respectively. The C 1s peak component at 286.2 eV is attributed to the C–O bond, indicating the formation of the hydroxyl groups on the MWCNT surface.

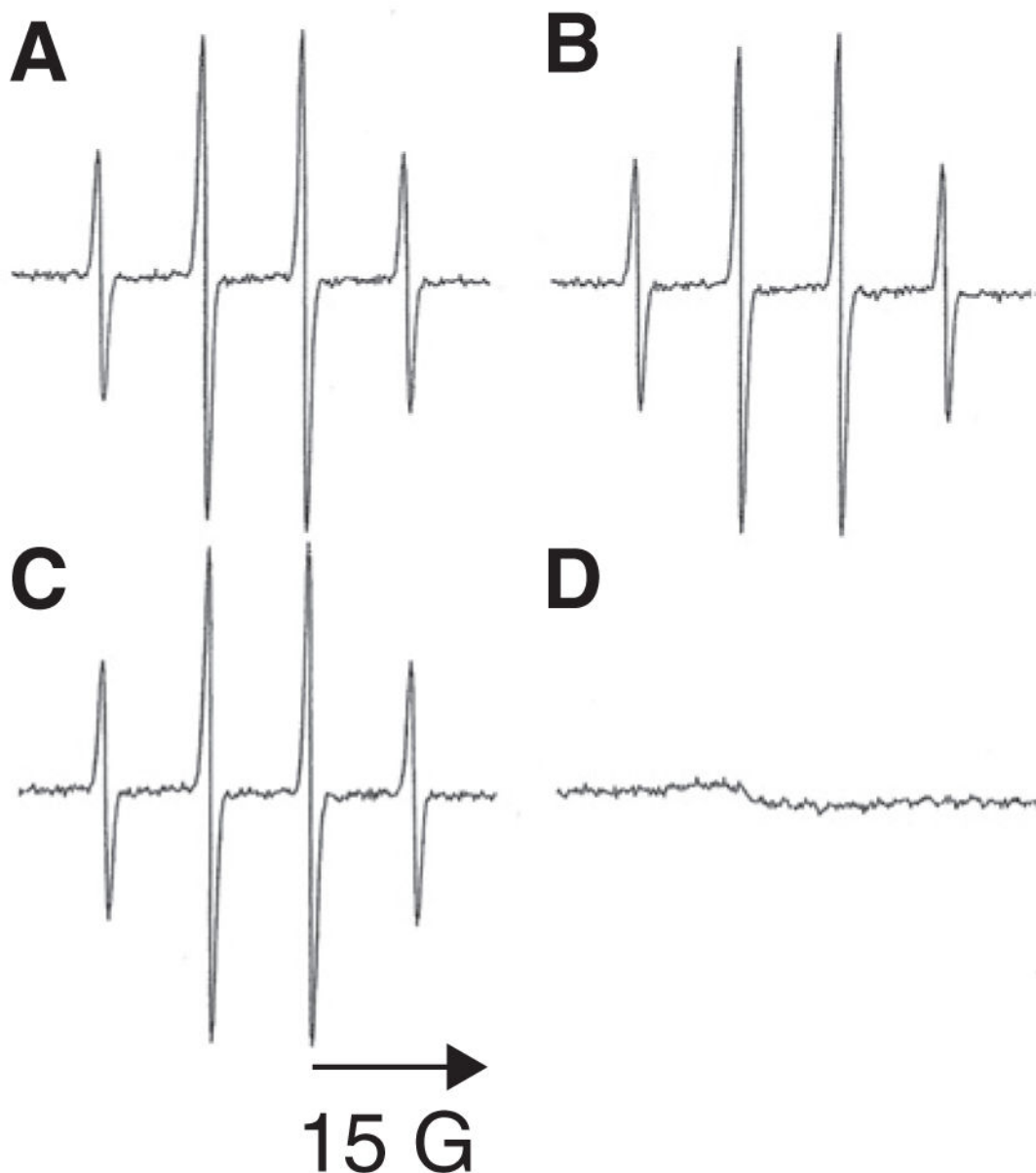


**Figure 3.**

ESR study of MWCNT. (Panel A) PBS with 100 mM DMPO + 0.1 mM  $\text{FeSO}_4$  + 1 mM  $\text{H}_2\text{O}_2$ . (Panel B) DM with 100 mM DMPO + 0.1 mM  $\text{FeSO}_4$  + 1 mM  $\text{H}_2\text{O}_2$ . (Panel C) DM with 100 mM DMPO + 0.1 mM  $\text{FeSO}_4$  + 1 mM  $\text{H}_2\text{O}_2$  + 0.8 mg/ml MWCNT. (Panel D) DM with 100 mM DMPO + 1 mM  $\text{H}_2\text{O}_2$  + 0.8 mg/ml MWCNT. All ESR spectra were obtained using the following settings: centre field = 3480 G, sweep width = 100 G, microwave frequency = 9.794 GHz, microwave power = 20.120 mW, receiver gain = 10,000 and signal channel time constant = 40.960 ms.

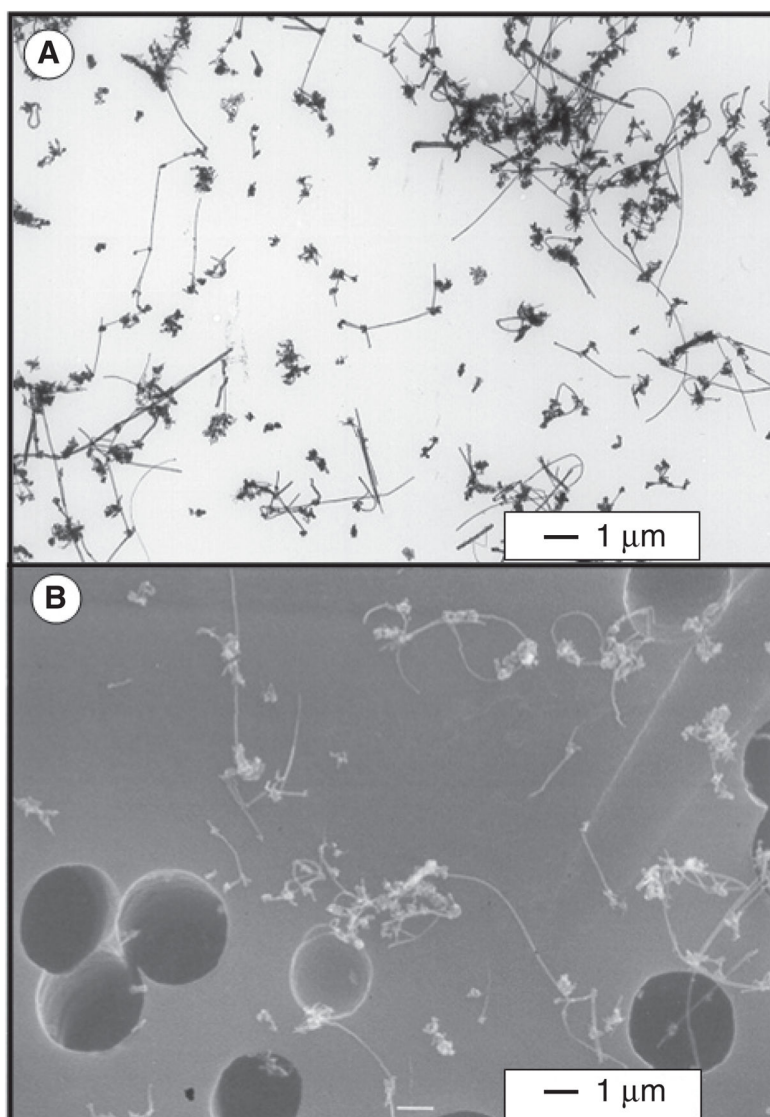


**Figure 4.** TEM and field emission SEM images of MWCNT aerosol samples. The exposure chamber samples were collected by drawing aerosol from the chamber through 47-mm polycarbonate filters (Whatman, Clinton, PA) at a rate of 1 L/min. (Panel A) TEM images were photographed on a JEOL 1220 transmission electron microscope. (Panel B) Field emission SEM images were obtained with a Hitachi S4800.

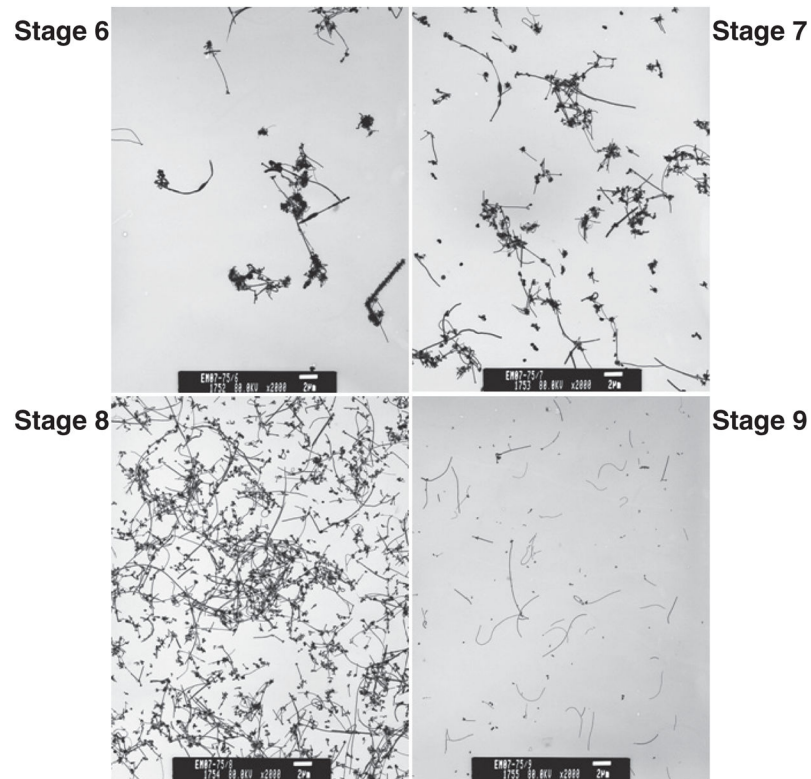


**Figure 5.** Transmission electron microscopy images of different stages in a MOUDI cascade impactor. The TEM images were used to determine count mode aerodynamic diameter of the MWCNT aerosol.

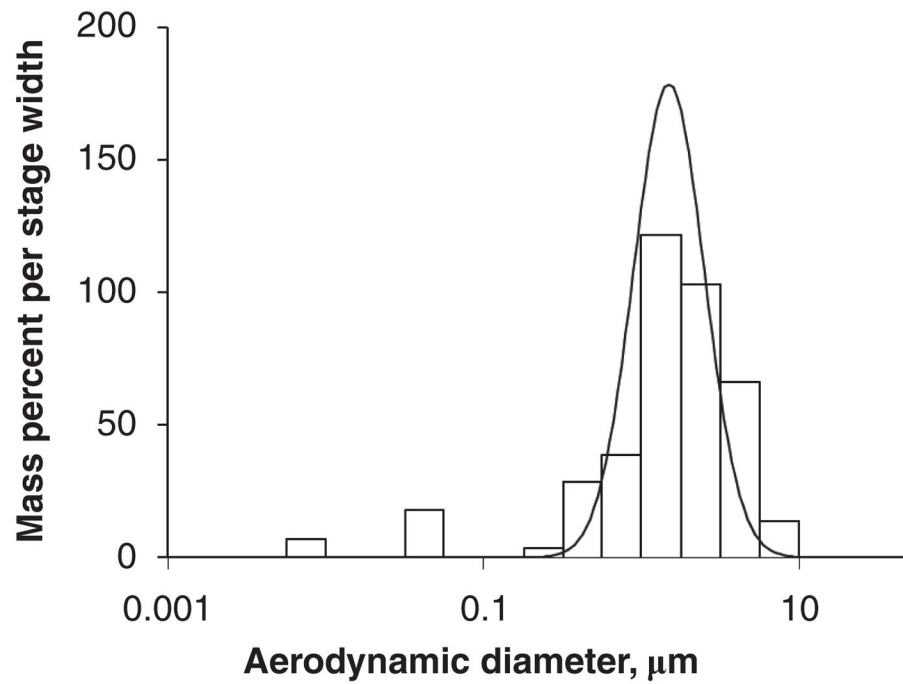


**Figure 6.**

A typical size distribution of the MWCNT aerosol in the exposure chamber ( $M$  = mass concentration and  $D_{ae}$  = aerodynamic diameter). The distribution has a MMAD = 1.5  $\mu\text{m}$  and a GSD of 1.67.

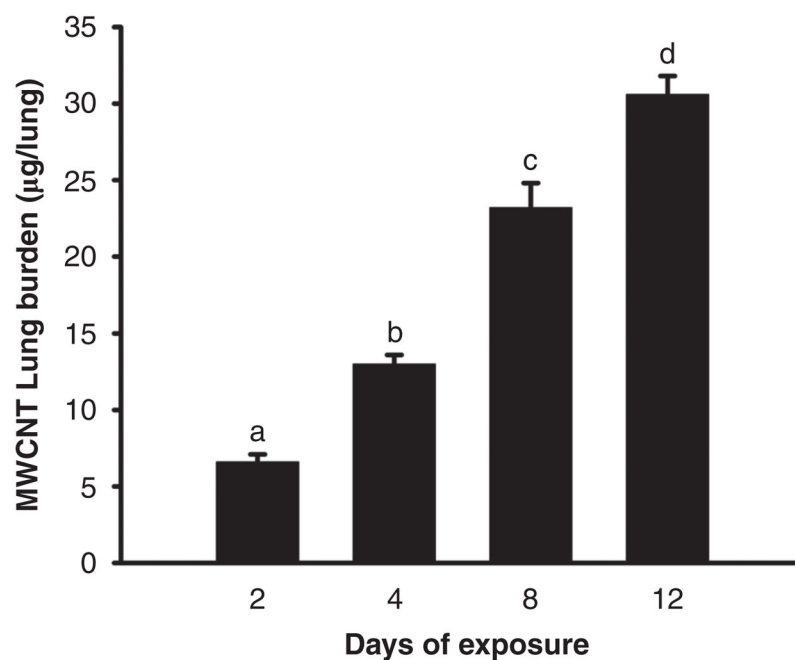


**Figure 7.** MWCNT lung burden. (a) 2 days exposure =  $16.6 \pm 1.3$  µg MWCNT, (b) 4 days exposure =  $32.5 \pm 1.6$  µg MWCNT, (c) 8 days exposure =  $58.0 \pm 3.9$  µg MWCNT, and (d) 12 days exposure =  $76.7 \pm 3.0$  µg MWCNT.

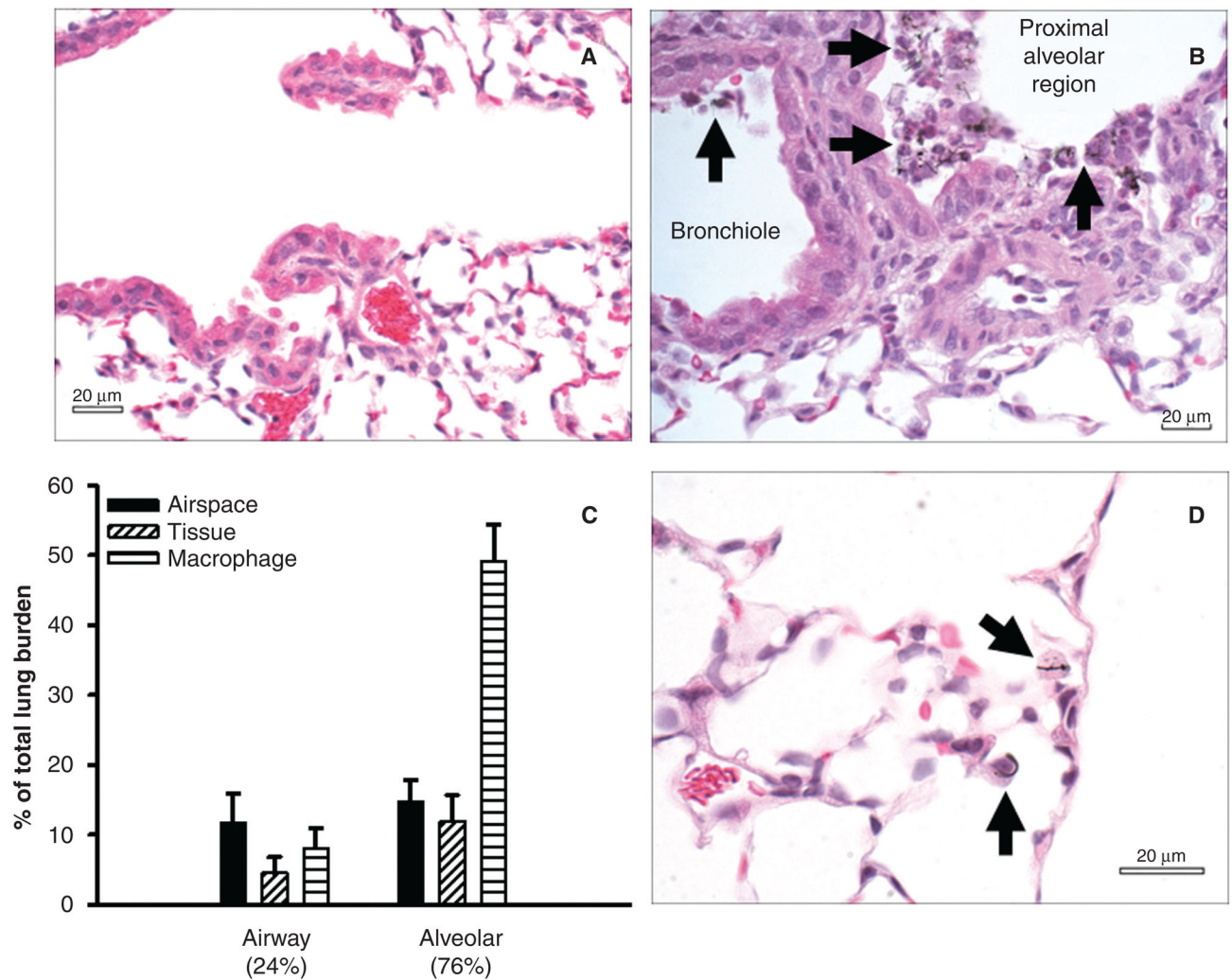


**Figure 8.**

Lung distribution of MWCNT. Mice were exposed by inhalation exposure to air or MWCNT (10 mg/m<sup>3</sup>) for 4 days and the lungs were collected at 1 day post-exposure. (Panel A) No MWCNT were observed in air-exposed controls. (Panel B) MWCNT were observed in the bronchioles and proximal alveolar region of MWCNT-exposed mice. (Panel C) Morphometric analyses of MWCNT distribution. Values are means  $\pm$  SE ( $n = 8$ ). (Panel D) MWCNT were observed at the pleural wall.

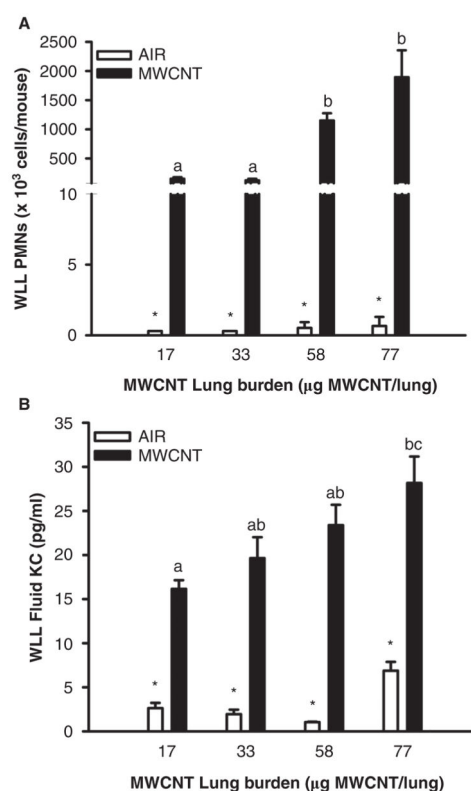


**Figure 9.**

Pulmonary inflammation and chemokine KC protein are induced by exposure to MWCNT. Mice were exposed by inhalation exposure to air (vehicle) or MWCNT (10 mg/m<sup>3</sup>) for 2, 4, 8 or 12 days. WLL studies were conducted at 1 day post-exposure. (Panel A) Pulmonary inflammation was assessed by determining WLL PMN. (Panel B) The chemokine KC, which is a neutrophil chemoattractant, was determined in first WLL fluid. Values are means  $\pm$  SE ( $n = 7-9$ ). Bars with different letters are significantly different ( $p < 0.05$ ). An asterisk indicates air-exposed controls were significantly lower ( $p < 0.05$ ) in comparison to the corresponding MWCNT-exposed group.

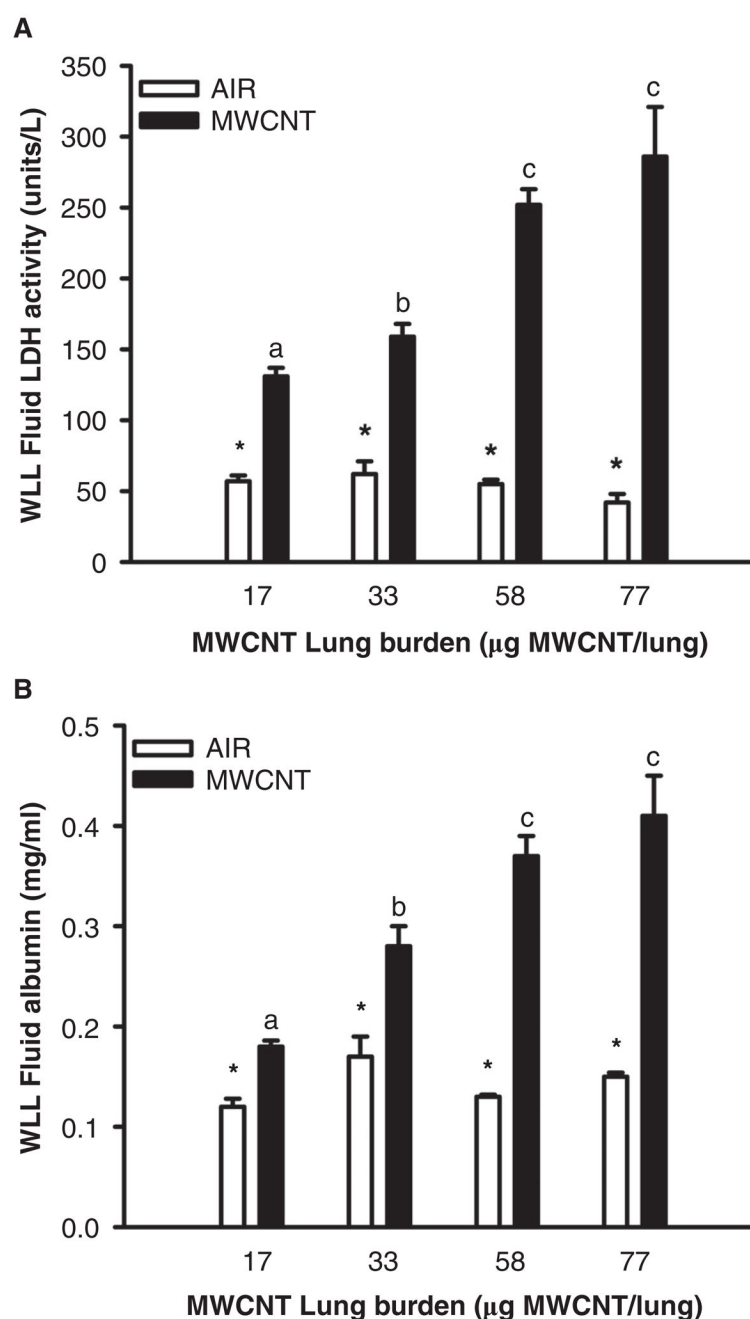


**Figure 10.**

WLL fluid LDH activities and albumin concentration. Mice were exposed by inhalation exposure to air (vehicle) or MWCNT ( $10 \text{ mg/m}^3$ ) for 2, 4, 8 or 12 days. WLL studies were conducted at 1 day post-exposure. (Panel A) WLL fluid LDH activities. (Panel B) WLL fluid albumin concentrations. Values are means  $\pm$  SE ( $n = 7-9$ ). Bars with different letters are significantly different ( $p < 0.05$ ). Asterisk indicates air-exposed controls were significantly lower ( $p < 0.05$ ) in comparison to the corresponding MWCNT-exposed group.

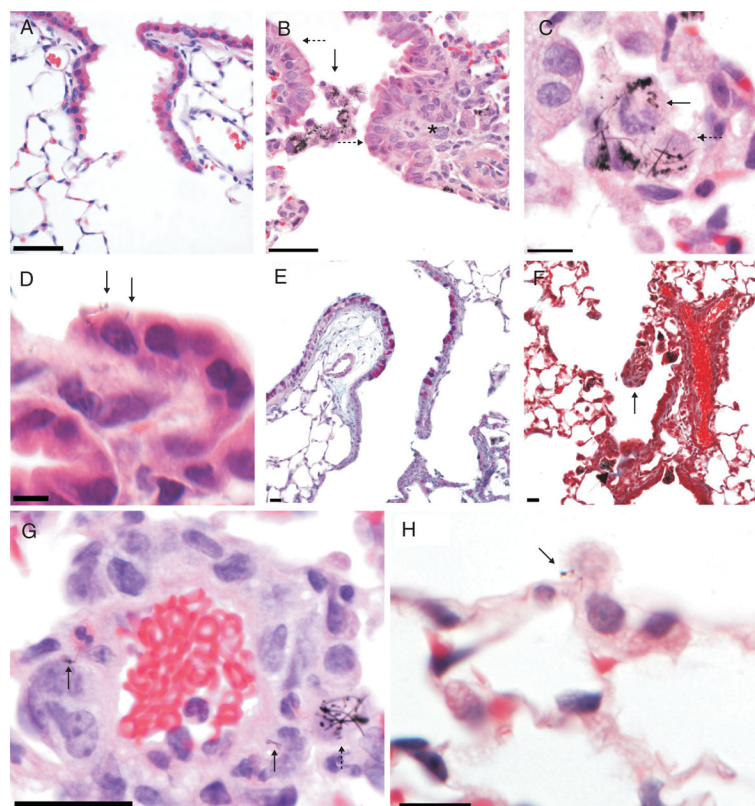


**Figure 11.**

Histopathologic changes in the lung of MWCNT-exposed mice. (Panel A) Mice exposed to air had normal histology at the bronchioloalveolar junction. Bar = 20  $\mu$ m. (Panel B) Mice exposed to MWCNT had hypertrophy and hyperplasia of the bronchiolar epithelium (dashed arrows), macrophages containing phagocytised MWCNT within the bronchiolar lumen, and interstitial and alveolar inflammation (\*) centered at the bronchioloalveolar junction. Bar = 20  $\mu$ m. (Panel C) Nuclear abnormalities in alveolar macrophages included loss of nuclear staining consistent with karyolysis (dashed arrow) and, in this section, something almost never seen in controls, an abnormal mitotic figure with an apparent association between MWCNT and chromatin (solid arrow). Bar = 10  $\mu$ m. (Panel D) A partially polarised section of bronchiolar epithelium shows intraepithelial MWCNT (solid arrows). Bar = 10  $\mu$ m. (Panel E) Alcian-blue/PAS stained sections of airway epithelium in the MWCNT-exposed mice revealed mucous metaplasia as demonstrated by magenta to purple cytoplasmic staining of mucosubstances. Bar = 20  $\mu$ m. (Panel F) Fibrosis (arrows) was usually bronchiolocentric, in foci of inflammation. Excess collagen deposition was demonstrated by blue staining in Masson's trichrome-stained sections. Bar = 20  $\mu$ m. (Panel G) Vasculitis with mural MWCNT (solid arrows). A macrophage at the margins of the *tunica adventitia* contains incompletely phagocytised MWCNT (dashed arrow). Bar = 20  $\mu$ m. (Panel H) Pleural penetration of MWCNT with phagocytosis of the pleural MWCNT. Bar = 10  $\mu$ m.

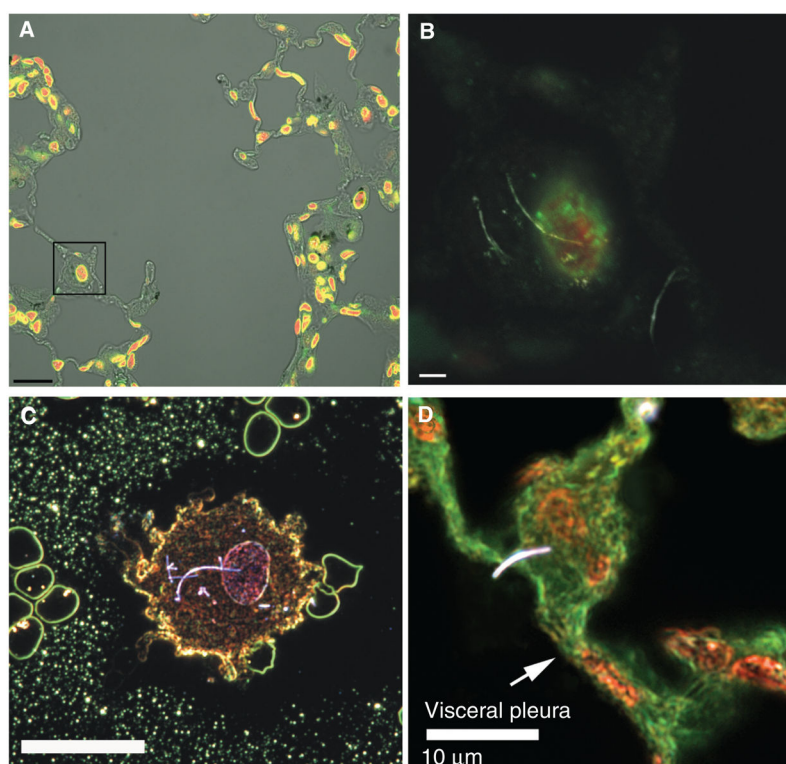


**Figure 12.**

Augmented microscopic imaging of lung after 12 days of MWCNT exposure. (Panel A) A confocal photomicrograph of lamin-B immunofluorescence and ethidium homodimer-1 staining of permeabilized cells localizes the alveolar duct region of the lung, while low-level transmitted light reveals occasional MWCNT deposited in the optical section. The MWCNT appear black due to blocking of transmitted light. Bar = 20  $\mu\text{m}$ . (Panel B) A confocal photomicrograph of an optical section of a reflected light image from the macrophage in the square of Panel A to demonstrate MWCNT, while multitracking allows demonstration of the nuclear envelope by green lamin B1 staining and nucleic acid by red ethidium homodimer-1 staining to localize the MWCNT that penetrates the nucleus. Bar = 2  $\mu\text{m}$ . (Panel C) Enhanced-darkfield light microscopic image of a cytospin slide showing a macrophage with a long MWCNT penetrating the nucleus. Bar = 20  $\mu\text{m}$ . (Panel D) Enhanced-darkfield light microscopic image showing pleural penetration by a MWCNT.

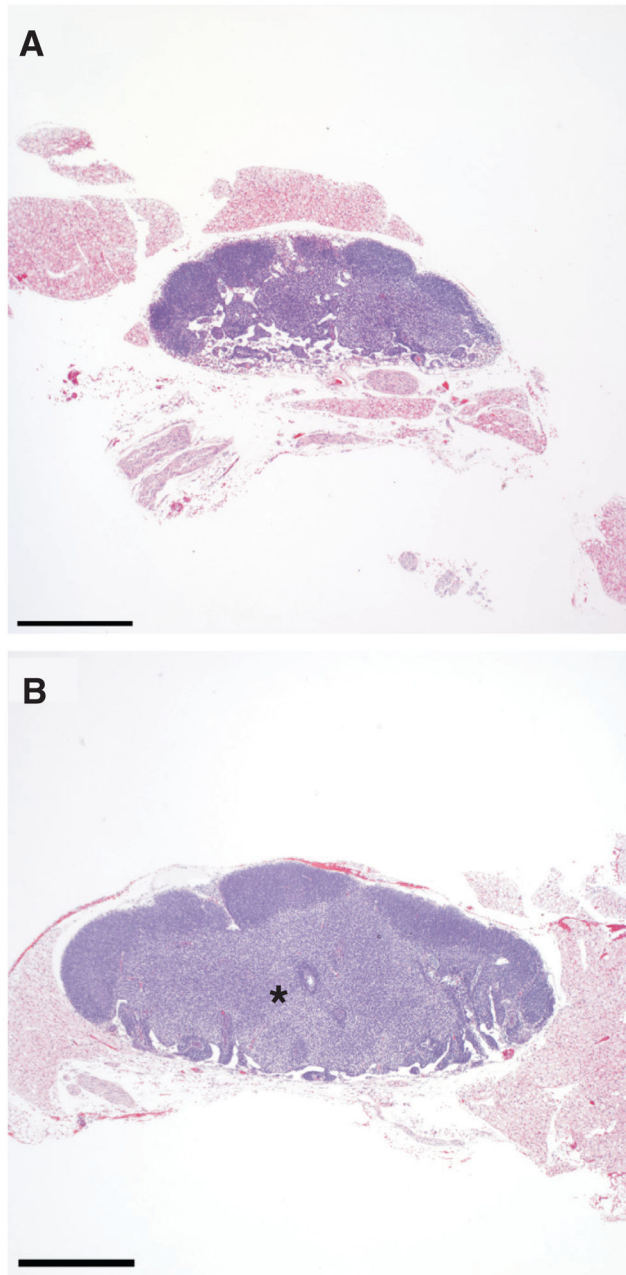


**Figure 13.**

Lymph node changes after MWCNT exposure. (Panel A) Tracheobronchial lymph nodes were within normal limits in air-exposed control mice. (Panel B) In MWCNT-exposed mice, lymph nodes were enlarged with hyperplasia principally localized to the deep paracortex (\*). Bar = 500 μm.

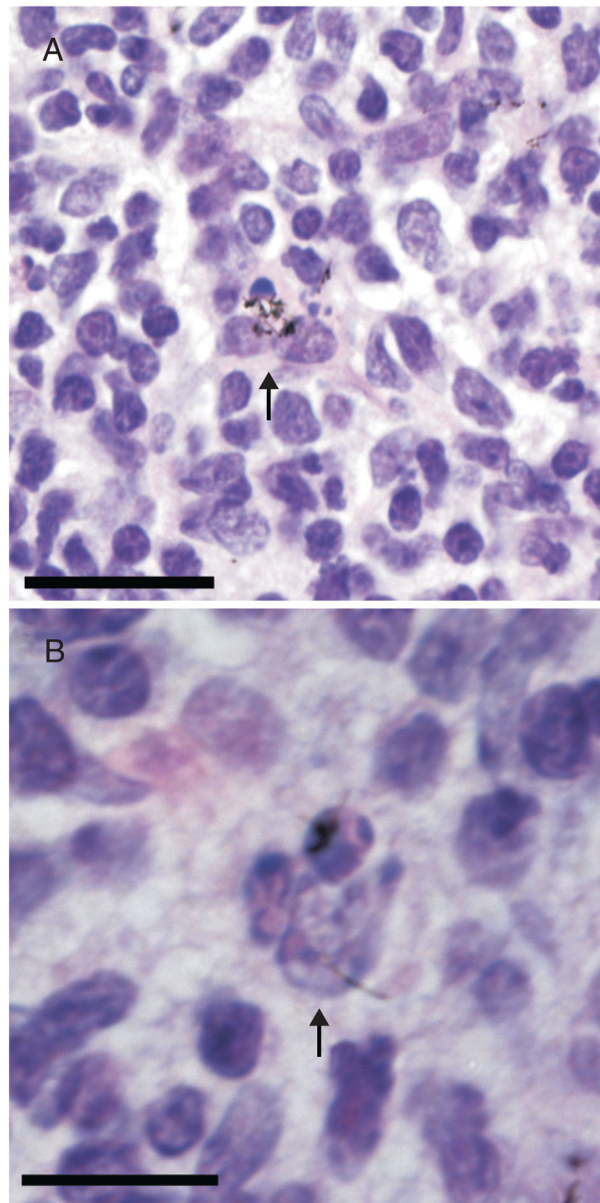


**Figure 14.**

Lymph node changes after MWCNT exposure. (Panel A) High magnification image of cells in the expanded lymph node para-cortex from a MWCNT-exposed mouse with intracytoplasmic MWCNT and nuclear debris (arrow). Bar = 20  $\mu\text{m}$ . (Panel B) Higher magnification partially polarized image of a macrophage containing nuclear debris and MWCNT. The partial polarisation facilitates demonstration of MWCNT but causes a slightly blurry appearance. A MWCNT appears to penetrate the nucleus and chromatin is clumped beneath the nuclear envelope. Bar = 10  $\mu\text{m}$ .

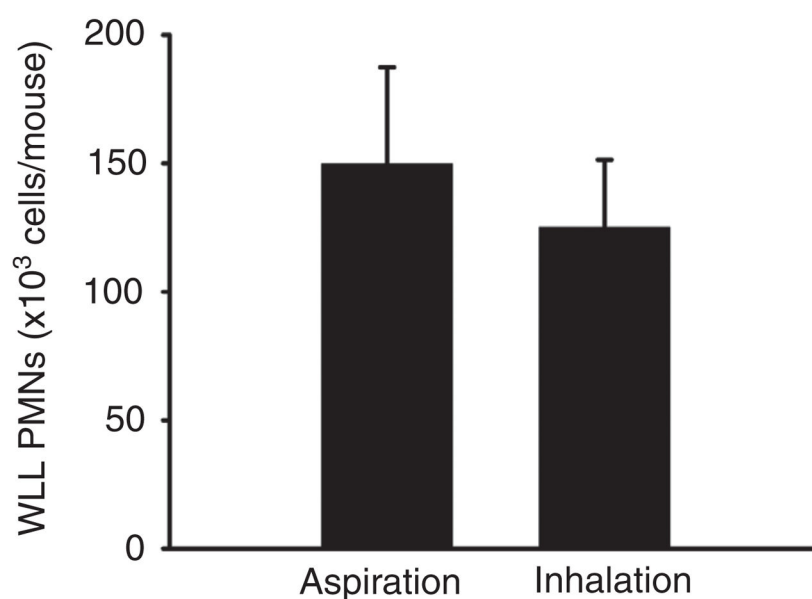


**Figure 15.**

Comparison of pulmonary inflammation induced by exposure to MWCNT by aspiration exposure (10  $\mu\text{g}/\text{mouse}$ ) or inhalation exposure (10  $\text{mg}/\text{m}^3$ , 4 days, MWCNT lung burden =  $13.0 \pm 0.6 \mu\text{g}/\text{lung}$ ) at 1 day post-exposure. Vehicle-exposed groups for aspiration study and inhalation study were  $0.75 \pm 0.37 \text{ PMN}$  ( $10^3 \text{ cells}/\text{mouse}$ ) and  $0.30 \pm 0.00 \text{ PMN}$  ( $10^3 \text{ cells}/\text{mouse}$ ), respectively. Values are means  $\pm$  SE ( $n = 7-9$ ).

Summary of pulmonary histopathology findings.

Table I

Exposure duration (days)	Exposure	Total <i>n</i>	Bronchioloalveolar inflammation	Fibrosis	Mucous metaplasia	Vascular changes	Bronchiolar epithelial hypertrophy and hyperplasia
4	Air	8	0 ( <i>n</i> = 8)	0 ( <i>n</i> = 8)	0 ( <i>n</i> = 8)	0 ( <i>n</i> = 8)	0 ( <i>n</i> = 8)
	MWCNT	8	5 ( <i>n</i> = 3) <sup>*</sup>	0 ( <i>n</i> = 7)	0 ( <i>n</i> = 1) <sup>*</sup>	5 ( <i>n</i> = 2) <sup>*</sup>	6 ( <i>n</i> = 2) <sup>*</sup>
8	Air	6	6 ( <i>n</i> = 5)	5 ( <i>n</i> = 1)	2 ( <i>n</i> = 4)	6 ( <i>n</i> = 6)	7 ( <i>n</i> = 6)
	MWCNT	6	5 ( <i>n</i> = 6) <sup>*</sup>	4 ( <i>n</i> = 2) <sup>*</sup>	5 ( <i>n</i> = 3) <sup>*</sup>	3 ( <i>n</i> = 2) <sup>*</sup>	5 ( <i>n</i> = 5) <sup>*</sup>
12	Air	6	0 ( <i>n</i> = 6)	0 ( <i>n</i> = 6)	0 ( <i>n</i> = 5)	0 ( <i>n</i> = 6)	0 ( <i>n</i> = 6)
	MWCNT	6	5 ( <i>n</i> = 4) <sup>*</sup>	5 ( <i>n</i> = 5) <sup>*</sup>	6 ( <i>n</i> = 6) <sup>*</sup>	5 ( <i>n</i> = 2) <sup>*</sup>	6 ( <i>n</i> = 6) <sup>*</sup>

Values represent histopathology score (severity + distribution) and inside parentheses the number of animals (*n*) with that score;

<sup>\*</sup> Significant difference between control and MWCNT exposure group.

**Table II**

Summary of histopathology findings in the tracheobronchial lymph node.

Exposure duration (days)	Exposure	Total <i>n</i>	Hyperplasia	MWCNT translocation
4	Air	8	0 ( <i>n</i> = 4)	0 ( <i>n</i> = 4)
			Not found ( <i>n</i> = 4)	Not found ( <i>n</i> = 4)
	MWCNT	8	0 ( <i>n</i> = 4)	0 ( <i>n</i> = 2)
			2 ( <i>n</i> = 2)	1 ( <i>n</i> = 5)
			3 ( <i>n</i> = 1)	Not found ( <i>n</i> = 1)
8	Air	6	0 ( <i>n</i> = 4)	0 ( <i>n</i> = 4)
			Not found ( <i>n</i> = 2)	Not found ( <i>n</i> = 2)
	MWCNT	6	2 ( <i>n</i> = 1)	2 ( <i>n</i> = 2)
			3 ( <i>n</i> = 1)	Not found ( <i>n</i> = 4)
			Not found ( <i>n</i> = 4)	
12	Air	6	0 ( <i>n</i> = 3)	0 ( <i>n</i> = 3)
			Not found ( <i>n</i> = 3)	Not found ( <i>n</i> = 3)
	MWCNT	6	3 ( <i>n</i> = 5)*	3 ( <i>n</i> = 5)*
			Not found ( <i>n</i> = 1)	Not found ( <i>n</i> = 1)

Values represent severity score (on a scale of 1 to 5) and inside parentheses the number of animals (*n*) with that score; A designation of not found is included because the ability to find a mouse tracheobronchial lymph node is influenced by the size of the lymph node;

\* Significant difference between control and MWCNT exposure group.

**Table III**

Summary of histopathology findings in the nose.

Exposure duration (days)	Exposure	Total <i>n</i>	Inflammation, level T1	Inflammation, level T2	Inflammation, level T3	Inflammation, level T4
12	Air	6	0 ( <i>n</i> = 6)	0 ( <i>n</i> = 5)	0 ( <i>n</i> = 6)	0 ( <i>n</i> = 6)
				2 ( <i>n</i> = 1)		
	MWCNT	6	0 ( <i>n</i> = 1)*	5 ( <i>n</i> = 1)*	4 ( <i>n</i> = 1)*	0 ( <i>n</i> = 2)*
			5 ( <i>n</i> = 4)	6 ( <i>n</i> = 5)	5 ( <i>n</i> = 3)	2 ( <i>n</i> = 1)
			6 ( <i>n</i> = 1)		6 ( <i>n</i> = 2)	5 ( <i>n</i> = 2)
						6 ( <i>n</i> = 1)

Values represent histopathology score (severity + distribution) and inside parentheses the number of animals (*n*) with that score;

\* Significant difference between control and MWCNT exposure group.